Mon. Not. R. Astron. Soc. **000**, 000–000 (0000) Printed 9 September 2008 (MN LATEX style file v2.2)

Correlations among the properties of galaxies found in a blind HI Survey, which also have SDSS optical data.

D. A. Garcia-Appadoo[1,4⋆], A. A. West[2,3], J. J. Dalcanton[3], L. Cortese[4] and M. J. Disney[4]

[1]*European Southern Observatory, Alonso de Cordova 3107, Casilla 19001, Vitacura, Santiago 19, Chile*
[2]*Astronomy Department, University of California, 601 Campbell Hall, Berkeley, CA 94720-3411, USA*
[3]*Physics-Astronomy Building C309, Department of Astronomy, University of Washington, Box 351580, Seattle, WA 98195, USA*
[4]*Physics & Astronomy Department, Cardiff University, 5 The Parade, Cardiff, CF24 3AA, UK*

arXiv:0809.1434v1 [astro-ph] 9 Sep 2008

Accepted. Received; in original form

ABSTRACT

We have used the Parkes Multibeam system and the Sloan Digital Sky Survey (SDSS) to assemble a sample of 195 galaxies selected originally from their HI signature to avoid biases against unevolved or low surface brightness objects. For each source 9 intrinsic properties are measured homogeneously, as well as inclination and an optical spectrum. The sample, which should be almost entirely free of either misidentification or confusion, includes a wide diversity of galaxies ranging from inchoate, low surface brightness dwarfs to giant spirals. Despite this diversity there are 5 clear correlations among their properties. They include a common dynamical mass-to-light ratio within their optical radii, a correlation between surface-brightness and Luminosity and a common HI surface-density. Such correlation should provide strong constrains on models of galaxy formation and evolution.

Key words: galaxies: fundamental parameters – galaxies: evolution – galaxies: general – galaxies: structure – galaxies: peculiar.

1 INTRODUCTION

Searching for systematic correlations among the global properties of galaxies, analogous to the H-R diagram for stars, may offer the best hope of having a better understanding about their formation and evolution. The recent availability of large and systematic datasets at several wavelengths makes this a good time to search. Such searches go back to the optical pioneers of galaxy exploration such as Hubble (1937), Holmberg (1965), de Vaucouleurs (1991) and Zwicky (1942). The trends and correlations they discovered, re-emerge very clearly in the Sloan Digital Sky Survey, as described by Blanton et al. (2003) in their analysis of 200.000 galaxies at redshifts of ~ 0.1.

This paper deals with a much smaller sample of galaxies, but ones found by an entirely different technique, i.e. in a blind search for neutral Hydrogen gas at 21-cm. The principal motivations for such a blind search are two. First of all, by definition, optically selected galaxies already contain many stars, which may not be the case in the younger, or less evolved galaxies, which may have the most to tell us about their formation and evolution. Apart from X-ray searches, which detect the very hot gas in the potential wells of giant ellipticals, most galaxy searches rely, either directly or indirectly, on the presence of stars and so are biased against young or unevolved objects. Secondly, a blind HI search offers a unique way round the strong optical surface brightness selection effects, which could disguise the very correlations one is looking for. By definition a galaxy must be separately both luminous enough *and* large enough to distinguish it above a sky background which, by galaxy standards, is quite bright. These two *separate* requirements squeeze optically selected galaxies into an extremely narrow range of surface brightnesses (SB) centred, for a given catalogue, on Σ_{cat} where:

$$\Sigma_{cat} \equiv \frac{l_{ap}}{\pi\theta_{ap}^2} \quad (1)$$

where l_{ap} and θ_{ap} are the minimum apparent luminosity, and the minimum apparent angular radius which the galaxy catalogue will accept (Disney 1999). The Full Width Half Maximum (FWHM) of the detectable range is typically only 3 magnitudes wide. Such a narrow stricture certainly impoverished the old photographic surveys (Disney 1976, Disney & Phillipps 1983, Dalcanton 1997). It might be naively thought that CCDs would have cured this stricture. Not so, because they detect galaxies that are both fainter *and* smaller than emulsions, their Σ_{cats}'s are (see equation (1)) scarcely any dimmer. On the other hand, the limitation with an HI-selected sample is that it will miss the early type galaxies - which contain very little neutral gas. According to the SDSS survey late types

⋆ E-mail: dgarcia@eso.org

make up the large majority of all galaxies, although they may emit less than their fair share of light (Blanton et al. 2001).

Blind HI surveys face four main problems. To reach sources of a given column density of HI (N_{HI} in atoms cm^{-2}) any survey must be at least sensitive enough to find them in the most favourable case, i.e. when they fill the beam. In that case (Minchin 2003, Disney 2008) t_{obs} (per beam) $\geqslant k/[N_{HI}\ (\mathrm{min})]^2$ where k is independent of dish-diameter D (because a larger dish projects the same system noise onto a smaller area of sky). Since there is a loose correspondence between N_{HI} and SB (e.g. Swaters et al. 2003). Mathematically:

$$N_{HI} \cong 10^{20.1} \left(\frac{M_{HI}}{L_B}\right)_{\odot} 10^{[0.4(27-\overline{\mu}_{21})]}\ atoms\ cm^{-2} \qquad (2)$$

(Disney & Banks 1997) where $\left(\frac{M_{HI}}{L_B}\right)_{\odot}$ is in solar units and $\overline{\mu}_{21}$ is the average SB in B mag arcsec^{-2}, taken over the same area as N_{HI}. Since the effective SB (μ_{eff}) of an exponential disc is 2.1 magnitudes brighter than $\overline{\mu}_{21}$ (Salpeter & Hoffman 1996) column density sensitivity at the $N_{HI} < 10^{19.5} cm^{-2}$ level is needed to detect LSBGs (i.e. μ_{eff} 25.0 B mag arcsec^{-2}) with $\left(\frac{M_{HI}}{L_B}\right)_{\odot} \approx$ 0.3 (see Section 3), which in turn requires integration times per beam of several hundred seconds - which rendered earlier blind HI surveys either too insensitive or too impractical to detect LSBGs. Since this difficulty was not recognised until recently, some earlier claims, based on small blind HI surveys, to set rigid upper limits to the amount of cosmic HI or the numbers of LSBGs in the Universe, must be set aside [e.g. Shostak 1977, Fisher and Tully 1981, Zwaan et al. 1997].

The coming of the Multibeam HI detector (Staveley-Smith et al. 1996) was essential to carry out such blind HI surveys. HIPASS, the HI Parkes All Sky Survey (Meyer et al. 2004) used the first multibeam system to survey the entire Southern Sky, and the north up to +25°. More than 4000 sources were identified in the Southern Sky alone. The Equatorial Survey, described in this paper, was initially part of HIPASS, but with an accelerated search so as to exploit the SDSS-DR2 optical data when it emerged. HIPASS sources are typically more than a degree apart which makes for a real challenge in obtaining complementary optical, and other data, simply because, before SDSS, each source required a separate observing campaign.

The strong clustering of galaxies, and of HI galaxies in particular, makes the identification of the source with an optical candidate quite challenging. This is true even when both 21-cm and optical velocities are known, for galaxy velocities are strongly clustered too. To be certain that every Parkes-detected source was correctly identified with its optical counterpart would require interferometric follow-up in every case - which is infeasible when one is dealing with hundreds of sources, as here. We have used interferometry, coupled with simulations, to be certain that only a handful of the remaining sources (less than 10) are still misidentified. This handful is too small to affect the main correlations.

The Equatorial Strip Survey (ES henceforth), reported on here, was a search through HIPASS cubes between declinations $-6°$and +10°. Thus 5780 deg^2 of HI data, in the velocity range between -1280 and +12700 km s^{-1}, were searched largely by eye to come up with 1107 sources (Garcia-Appadoo PhD Thesis 2005). The Equatorial Strip was chosen because: (i) it was approximately perpendicular to the Galactic Plane and so it is mostly dark enough to make LSBGs detectable; (ii) it is accessible for follow up with a large range of instruments including the VLA, and for some of its area the SDSS-DR2; (iii) it includes the area searched for LSBGs by Impey et al. (1996) using the APM machine (Cawson et al. 1987) to scan UK-Schmidt plates. This should eventually lead to an estimate of the number of LSBGs still missing from wide-scale optical surveys. So long as LSBGs remain a putative reservoir for missing baryons (e.g. Fukugita et al. 1998) it is important to know this. Of the ES area, 50 per cent will eventually be scanned by SDSS, and 35 per cent of it is already publicly released. We concentrated our search in the 1700 deg^2 of the ES released earlier in DR2 (Abazajian et al. 2004). 370 cross identifications were made, and then refined down to only 195 to reduce possible misidentifications to a minimum. These 195 sources have SDSS-DR2 optical diameters (50 per cent light diameter and 90 per cent light diameter) between 0.16 and 6 arcmins (West et al. 2008). The SDSS pipeline photometry on sources of this size was known to be extremely unreliable so we had to devise new techniques to reduce the data (West PhD Thesis 2005), which delayed the project by nearly two years. Eventually we will analyse many more ES sources already observed with SDSS. But the results found for the first 195 are clear and interesting enough to merit being published now.

We have measured, at 21-cm, the peak flux, the integrated flux, the line width, and the spectral shape (e.g. two horned or Gaussian mainly), and in the optical the luminosities at u, g, r, i, z, two radii $R_{50}(g)$ and $R_{90}(g)$ containing respectively 50 and 90 per cent of the g-band light, the inclination, the morphology and a fibre nuclear spectrum set either on the nucleus or the brightest HII region. Given the strong correlations between some of the colours this amounts to about a dozen independent measurements, not far short of the 14 desired. Chiefly missing is a rotation curve to spell out the distribution of Dark Matter. Nevertheless we have sufficient information to hope that some important aspects of galaxy systematics will emerge. With 13 properties there will be $\sim (13\times12)/2 \sim$ 80 possible correlations to look for.

The previous largest survey of discs was reported in a remarkable, but largely unremarked paper by Gavazzi et al. in 1996 entitled *The phenomenology of disc galaxies*. They found: (a) the mass-to-light ratio in the NIR is virtually constant and equal to 4.6 in H-band solar units; (b) Population I indicators are all anti-correlated with mass; (c) Conversely the luminosity and surface brightness of old stellar populations all increase with mass; (d) Bulge components all increase non-linearly with mass; (d) All the above properties are independent of either morphological type or environment.

Previous blind HI surveys, with follow-up optical or NIR data, have been carried out by Zwaan et al. (1997), Spitzak and Schneider (1998), Rosenberg and Schneider (2000), Minchin et al. (2003), Davies et al. (2004), Giovanelli et al. (2005). Some of the results are discussed in Rosenberg et al. (2005), Rosenberg and Schneider (2003) and Minchin et al. (2004). The main results can be summarised briefly as follows:

(i) all but one galaxy (Minchin et al. 2005, 2007) seem to have optical counterparts;

(ii) although spirals predominate, the counterparts cover a wide variety of morphological types and luminosities;

(iii) there are significant, but not overwhelming, numbers of low surface brightness galaxies;

(iv) to within the measurement errors all HI galaxies have the same HI column densities ($\sim 10^{20.65\pm0.38} cm^{-2}$) and this is not a selection effect.

The various surveys differ from one another partly in radio sensitivity, but mainly in the quality of their optical or NIR follow-up data. Our Equatorial Survey is distinct in two main respects: a) we have been fastidious in rejecting all sources where there might be

more than one galaxy in or near the beam; b) we have available high quality multi-band SDSS-DR2 data for every source, data which is both sensitive and uniform, across a wide dynamic range. Rosenberg at al. (2005) have attempted a similar analysis using, instead of optical, 2MASS J-band data.

Our most interesting results can be summarised as follows: a) All galaxies have the same mass-to-light ratio in H-band solar units. In other words Gavazzi's Law holds over a dynamic range of 8 mag in absolute luminosity even in HI-selected galaxies free of optical selection effects. b) There is a clear correlation between SB and Luminosity. Combined with (a) it reveals a correlation between dynamical mass and optical radius cubed, again over a large dynamic range, but now with more scatter. In other words there is roughly constant global-density for galaxies ($\sim 1 \times 10^{-24}\ gm\ cm^{-3}$). The Virial Theorem then implies the same angular velocity $\sim 4 \times 10^{-16}\ radians\ s^{-1}$, implying they could have rotated no more than 40 times in a Hubble epoch. (c) All the galaxies have the same global surface density in HI, that is to say the same HI-mass divided by optical-radius squared (R^2); (d) All the galaxies have exponential profiles throughout most of their extents so that R_{90} is correlated very tightly with R_{50}; (e) There is a clear colour-luminosity correlation in the sense that more luminous galaxies are redder, which is well known in optically selected samples.

The remainder of this paper is arranged by section as follows:

(2) *The Radio Observations* describe the HI survey, the detection process and the contents of the resulting catalogue.

(3) *The Optical Observations* looks into the sensitivity of the SDSS for picking up large angular-size low surface brightness galaxies, and galaxies with low $\left(\frac{M_{HI}}{L_B}\right)$ ratios. It then discusses the general problem of identifying reliable optical counterparts to HI sources in blind HI surveys.

(4) *The Diversity of Sources* displays complete data sets for a handful of detected objects, ranging from giant spirals to inchoate low surface brightness galaxies, which represent important HI-selected class types. A montage of the optical counterparts illustrates their very wide variety. Finally the complete data set is laid out in the form of tables.

(5) *The Correlations in Galaxy Properties* reveals the 5 separate correlations among their properties.

(6) *The Discussion* argues that the correlations, despite the small size of the sample, are significant, not unduly affected by distance uncertainties, and compatible with the Tully-Fisher relation: Line-width $\sim L^{\alpha}$, provided $\alpha \simeq 1/3$. If no more than 6 physical invariants control galaxies, as we argue, then 5 correlations suggest a degree of organisation among gas-rich galaxies which is surprising, and which must strongly constrain theories as to their formation and evolution.

2 THE RADIO OBSERVATIONS

The observations were carried out with the Parkes 64-meter radio telescope using the Multibeam System (Staveley-Smith et al. 1996) in which 13 adjacent beams employing 26 receivers track the sky at a rate of 1 degree per minute, returning several times to the same piece of sky weeks apart to minimise interference. The main characteristics of the survey are listed in Table 1.

The HIPASS catalogue, that is to say the pipeline catalogue of sources based on this raw data, has been released over the years using techniques, and with results described in Barnes et al. (2001), Meyer et al. (2004), Zwaan et al. (2004) and Wong et al. (2005).

Parameter	HIPASS value
Sky Coverage	$\delta < +25^{\circ}$
Integration time per beam	450 s
Average FWHM	14.3 arcmin
Gridded FWHM	15.5 arcmin
Pixel size	4 arcmin
Velocity range	-1280 to 12700 km s^{-1}
Channel Separation	13.2 km s^{-1}
Rms noise	13 mJy beam^{-1}
3σ HI Mass Limit[a]	$10^6\ D^2_{Mpc}\ M_{\odot}$
N_{HI} limit[a]	7.8×10^{18} cm^{-2}

[a] For ΔV = 100 km s^{-1}

Table 1. Summary of HIPASS survey parameters

Our Equatorial Survey, based on the same raw data, but covering only 5700 deg^2 around the Equator (Garcia-Appadoo, PhD Thesis, 2005) was analysed much earlier (1999) with the intention of providing an early source list in time for SDSS-DR2 release. Although it used almost identical search methods to HIPASS, and indeed copies most of them directly, it appears marginally more sensitive than the HIPASS catalogue of the same region (Wong et al. 2005), perhaps because we had more time to follow up marginal detections with the more sensitive narrow-band system at Parkes (Zwaan et al. 2004) thus winning fainter signal from noise. The Equatorial Survey (ES hereafter) covers 14 per cent of the entire sky in a band right round the celestial equator from declination -6°to +10°. Of this area about 1700 deg^2 is covered by the 2nd Data Release of the SDSS (Abazajain et al. 2004) which we will use as our source of optical information. Fig. 1 shows the distribution of sources around the sky, both those with SDSS-DR2 optical data and those without. The gaps caused by the Galactic Plane, as well as the strong peak at an R.A. of $\sim$ 12 hours due to the southern extension of the Virgo cluster are easily visible, note that the source at 20h R.A. lies in an additional small area of SDSS-DR2 coverage that, due to its small size, is not shown in Fig. 1. Fig. 2 shows the distributions of ES sources in both peak and integrated flux. As can be seen the distributions for both the ES sample with (hashed) and the sample without (clear) optical data are very similar. This indicates that the optical sub-sample we will be analysing here is representative of the sample as a whole and hence can be used to characterise the properties of HI selected galaxies in general.

The noise in the Parkes Multibeam data is complex, consisting of a mix of receiver noise, solar side-lobe emission, confusion and ripple in the 21-cm spectra with a characteristic frequency of $\sim$ 1200 km s^{-1} due to standing waves with the wavelength of 52 meters set up between the dish surface and the prime focus cabin by continuum sources in the beam. With such complex noise the selection effects which enter into the discrimination of weak sources cannot be anticipated, and must be recognised retrospectively. Multibeam data is presented to the observer in cubes with axes in the R.A., declination and radial-velocity directions. The cubes are 8 degs on a side separated into 4 arcmin pixels and divided in the third dimension into 1024 velocity channels each 13.1 km s^{-1} wide. Given that the original radio beam was 7 arcmin half-maximum in diameter the pixel signals are partially correlated, as are the velocity channels which have been Hanning-smoothed to 18 km s^{-1}. These cubes (102 of them in our case) were searched individually using a mixture of numerical algorithms and the eye-brain system. Algorithms are helpful, particularly in reducing labour; but none has so far proved anywhere as reliable or sensitive as the eye-

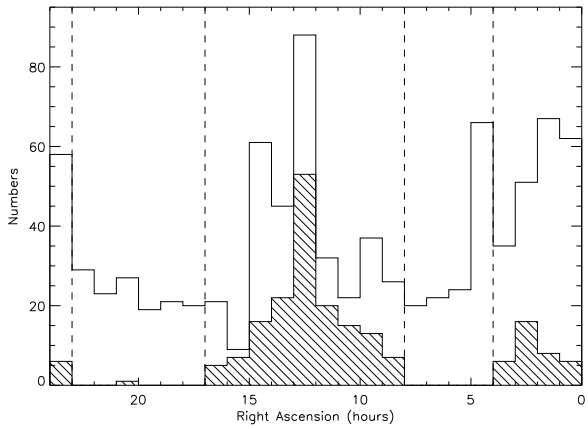

(a) Distribution of R.A.'s

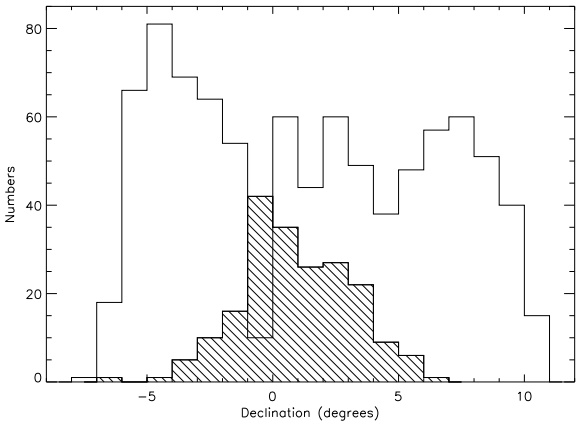

(b) Distribution of Declinations

Figure 1. Spatial distribution of the ES sample. (a) shows the distribution in right ascension. The dashed lines indicate the range where there is no optical SDSS-DR2 data available. (b) shows the distribution of ES sources in declination. The unfilled histogram indicates those HI sources without optical SDSS-DR2 data and the line-filled histogram the sources with optical SDSS-DR2 data.

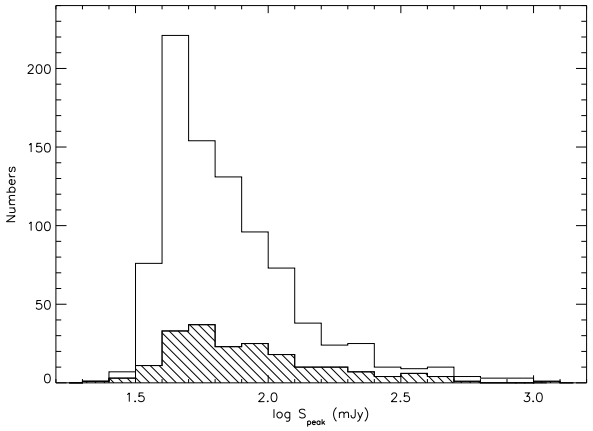

(a) Distribution of peak fluxes (S_{peak})

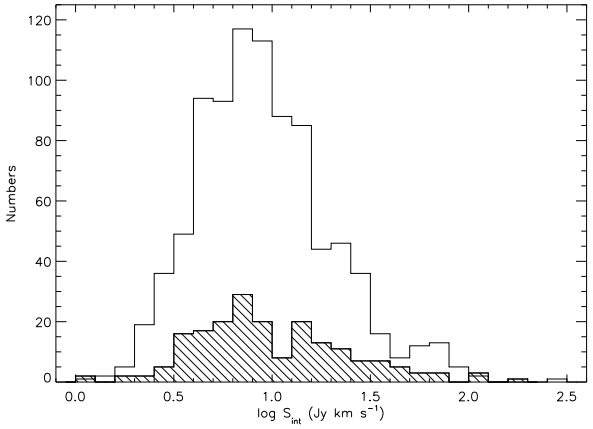

(b) Distribution of integrated fluxes (S_{int})

Figure 2. Flux distributions for the ES sample. The unfilled histogram indicates those HI sources without optical data and the line-filled histogram the sources with optical SDSS-DR2 data.

brain (e.g. Kilborn 2002). Each cube can be represented in 3 combinations (α, δ), (α, V) and (δ, V) where V is the radial velocity, and all 3 are searched before deciding a source is probably present. Such probable sources can be followed up by using the multibeam system in a more sensitive narrow-band mode. A combination of much higher velocity resolution (1.3 km s^{-1} per channel) and the ability to integrate indefinitely on a possible source, rather than for a total of 450 seconds in the scans, is a powerful filter against spurious misidentifications (Zwaan et al. 2004). Note that the existence, or otherwise, of an optical counterpart is in no sense used in selecting or rejecting a source, making the survey truly blind.

The ES HI sample was selected using methods almost identical to HIPASS selection (Meyer et al. 2004, Zwaan et al. 2004). The noise is complex so the only way to establish the likely reality of sources is to follow up a sufficient proportion with the more sensitive 'Narrowband System'. The hundreds of putative HIPASS sources followed up gives confidence that significantly less than 5% of the remaining ES sources could be spurious, far too small fraction to affect the correlations we are searching for [Section 5].

Fig. 3 shows the integrated flux as a function of the velocity width of the sources. It appears that detection by integrated flux

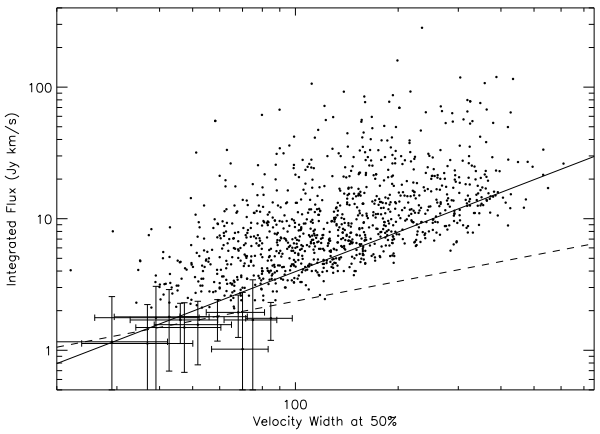

Figure 3. Selection limits in Velocity Width-integrated flux space. The theoretical 3σ limit for selection based on S$_{int}$ (constant signal-to-noise) is shown by the dashed line and the 3σ limit for S$_{peak}$ selection ($\frac{S_{int}}{\Delta V_{50}}$) is shown by the solid line. Most error bars have been omitted for clarity.

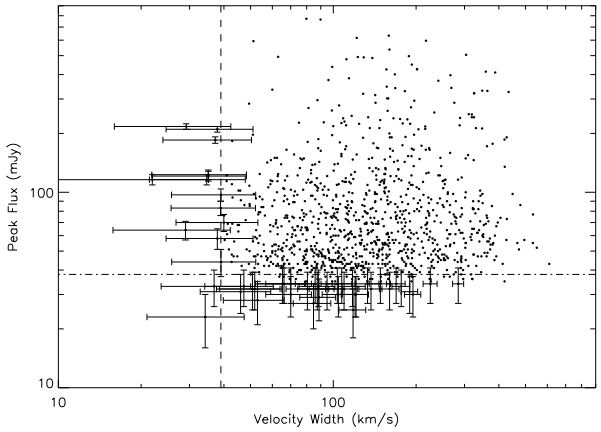

Figure 4. Selection limits in velocity width-peak flux space. The 3σ (39 mJy) shown here (dot-dashed line) can be seen to be a good match to the selection limit of the data. The dashed vertical line shows ΔV_{50} = 3 channels (39.6 km s^{-1}). Most error bars have been omitted for clarity.

is dependent on line width, with broad line sources being harder to find in the noise. In peak flux however it is much easier to set a clean selection criterion independent of line-width (see Fig. 4), as Kilborn (2002) and other searchers in the multibeam data have found.

Fig. 5 shows flux limited curves $N(S) \sim S^{-5/2}$ filled to peak fluxes (a) and integrated fluxes (b). Fig. 5(a) is suggestive of a peak-flux completeness limit $\sim$ 50 mJy.

The raw velocities are corrected for solar motion relative to the Local Group. The resulting distribution of radial velocities is shown in Fig. 6. Approximate distances are derived in a similar way as in Koribalski et al. (2004), using $D = v_{LG}/H_0$, where $v_{LG} = v_{sys} + 300\ sin\ l\ cos\ b$, H_0 = 75 km s^{-1} Mpc^{-1} is assumed throughout (and where necessary a cosmology with Ω_M = 0.3 and Ω_Λ = 0.7).

The HI masses were derived from the integrated fluxes using fitting processes identical to HICAT and:

$$M_{HI}(M_\odot) = 2.36 \times 10^5 \times D(Mpc)^2 \times \int S(HI)\, dV \qquad (3)$$

where D is the distance in Mpc and the integral $\int S(HI)dV$ is the integrated flux in Jy km s^{-1}, equation (3) assumes that all the sources are optically thin and that the upper levels of the 21-cm transition are fully excited. Fig. 7 shows the distribution of HI masses for the ES sample.

Although in this paper we are not going to try and compensate for HI selection effects we need to be aware of how they may have shaped our sample. The first worry concerns column-density-sensitivity. Will we have sufficient sensitivity to pick up LSBGs with correspondingly low N_{HI} (see equation (2))? It can be shown (Minchin et al. 2003) that the column-density-sensitivity, N_{HI} (cm^{-2}) , of any survey can be worked out retrospectively from the fluxes F (Jy km s^{-1}) and sizes $\delta\theta$ (HI diameter in arcmin) of the faintest sources within it according to:

$$[N_{HI}]_{min} = 4.5 \times 10^{20} \left(\frac{FHI}{\Delta V\ \delta\theta^2}\right)^{gal}_{min} \times\ \Delta V\ \frac{atoms\, km}{cm^2\ sec} \qquad (4)$$

where ΔV is their velocity width in km s^{-1}. This is the HI equivalent of equation (1) in the optical. For the ES it corresponds to $\sim 10^{19}$ cm^{-2}, or a low SB limit, according to equation (2), where $\overline{\mu}_{21}$ is the mean SB inside the 21-cm area of the galaxy:

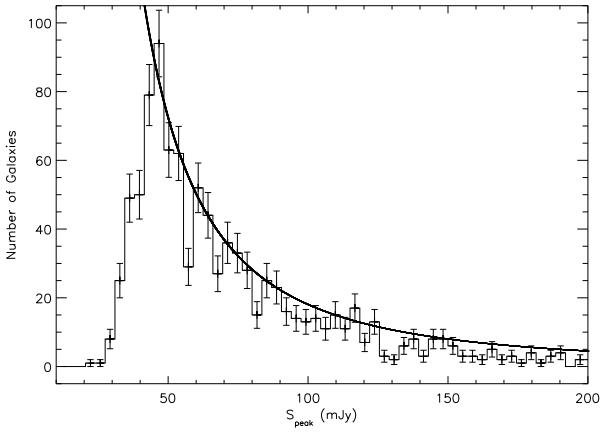

(a) Numbers of the ES sample by peak flux (S_{peak})

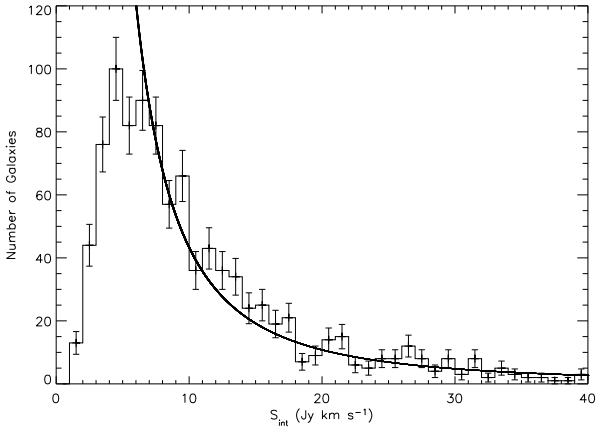

(b) Numbers of the ES sample by integrated flux (S_{int})

Figure 5. (a) Source count against peak flux. The histogram shows the numbers found in each bin of peak flux. (b) the completeness of the ES sample in integrated flux. The histogram shows the numbers found in each bin of peak flux. The curve in both panels represents $N(S) \sim S^{-5/2}$ as expected for a flux-limited survey.

$$\overline{\mu}_{21}(B) = 27 - 2.5 \log \left[\frac{N_{HI}}{10^{20.1}}\ /\ \left(\frac{M(HI)}{L_B}\right)\right]\ \frac{mag}{arcsec^2} \qquad (5)$$

For a typical $(M_{HI}/L_B) \sim 1$ this corresponds to a central SB μ_0 (B) $\sim$ 25.7 or an effective SB μ_{eff} (B) $\sim$ 27.5 which is very dim, dimmer than any optical catalogue covering a significant area (see Table 3 for definition of different SB's). Indeed it is so dim that one might question whether the SDSS could reach it. But here enters a surprising result recently discovered by Minchin using the Parkes multibeam to carry out a much deeper HI survey (HIDEEP; 9000 s beam^{-1}) of a small area, and with full optical follow up (Minchin et al. 2003). Despite its great sensitivity to low column densities ($N_{HI} \geqslant 2\times10^{18}$ atoms cm^{-2}) they found that there are no low column density galaxies. Indeed they found that all HI selected galaxies have, to within the errors, the same column density [$\sim 10^{20.5}$ cm^{-2} if spread over 5 effective radii, as in optically selected samples (Salpeter & Hoffman 1996)], see Fig. 8. We find the identical uniformity of N_{HI} in the ES, see Fig. 11(a).

Whatever the reason for Minchin's strange law (Minchin et al. 2003), and it needs explaining, the dimmest LSBGs we can expect to encounter in the ES will have, according to equation (5), and the fact that $\overline{\mu}_{eff} = \overline{\mu}_{21} - 2.1$ mag for an exponential disc:

Table 2. HI properties of the ES sample

ES Name	RA (J2000)	Decl. (J2000)	S_{peak} (Jy)	S_{int} (Jy km s^{-1})	v$_{sys}$ (km s^{-1})	W$_{20}$ (km s^{-1})	D (Mpc)	log M$_{HI}$ (M$_\odot$)
(1)	(2)	(3)	(4)	(5)	(6)	(7)	(8)	(9)
HIPEQ0014-00	00 14 36	-00 44 42	0.075	17.18	3914	290	50.9	10.02
HIPEQ0027-01a	00 27 47	-01 09 39	0.039	6.60	3848	223	54.2	9.66
HIPEQ0033-01	00 33 22	-01 07 01	0.131	17.24	1972	146	30.1	9.57
HIPEQ0043-00	00 43 31	-00 06 49	0.064	13.81	4124	287	60.6	10.08
HIPEQ0051-00	00 51 57	-00 28 25	0.117	14.84	1616	173	26.0	9.37
HIPEQ0058+00	00 58 50	00 37 46	0.048	4.97	5338	156	75.4	9.82

NOTE.– An extract of the table is shown here for guidance. It is presented in its entirety in the electronic edition of the Journal.

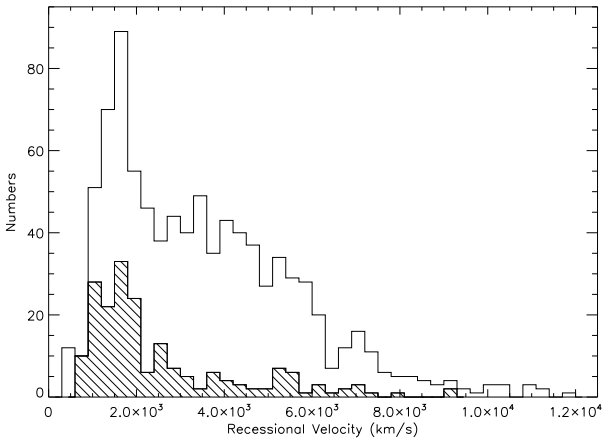

(a) distribution of recessional velocities

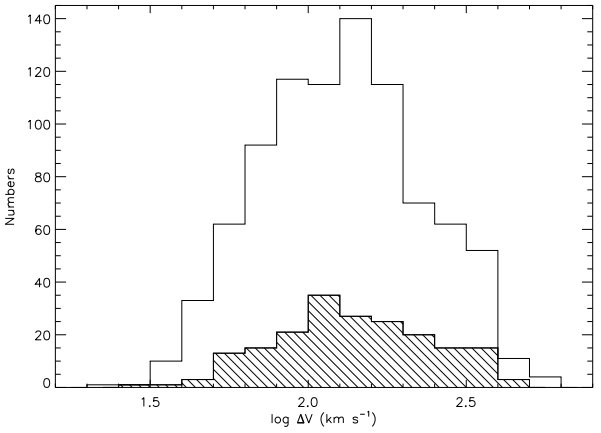

(b) distribution of velocity widths

Figure 6. (a) shows the recessional velocity distribution of the ES sample. (b) shows the distribution of the 50% velocity widths (ΔV_{50}) for the ES sample. The unfilled histogram indicates those HI sources without optical data and the line-filled histogram the sources with optical SDSS-DR2 data.

$$\mu_{eff}(B)(mag) = 23.9 + 2.5 \log\left(\frac{M(HI)}{L_B}\right) \quad (6)$$

which should be comfortably accessible with SDSS for galaxies with $(M_{HI}/L_B)_\odot < 5$ (see Section 3).

The HI properties obtained for the ES sample are listed in Table 2, which is provided in full in the electronic edition of this journal. The columns are as follows:

Column (1).– ES source name.

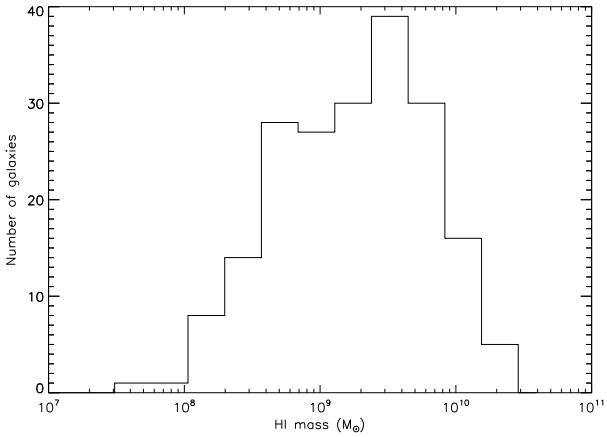

Figure 7. Distribution of HI masses for the ES sample

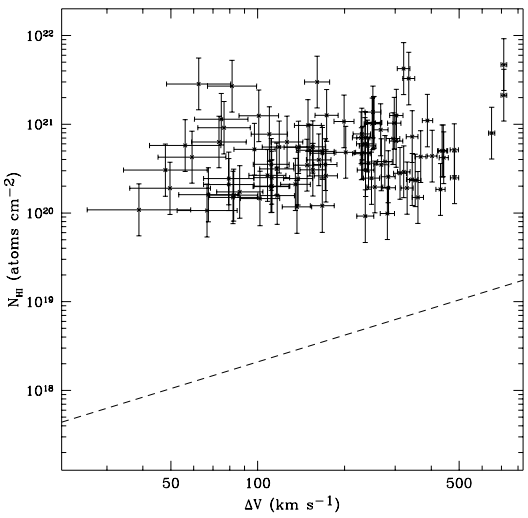

Figure 8. The distribution of the N$_{HI}$ column densities among the ∼100 HIDEEP galaxies observed by Minchin et al. (2003). The dashed line shows the sensitivity limit. There appear to be no low column density objects

Column (2) and (3).– Fitted HI positions in right ascension and declination (J2000).

Column (4).– HI peak flux density, S$_{peak}$.

Column (5).– Integrated HI flux density, S$_{int}$.

Column (6).– HI systematic velocity, v$_{sys}$, measured at the 20% level of peak flux density.

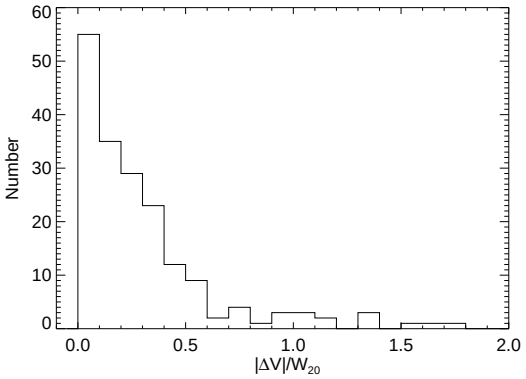

Figure 9. Distribution of velocity differences $\Delta V/W_{20}$ between radio sources and their optical counterparts in the ES for the original 310 sources.

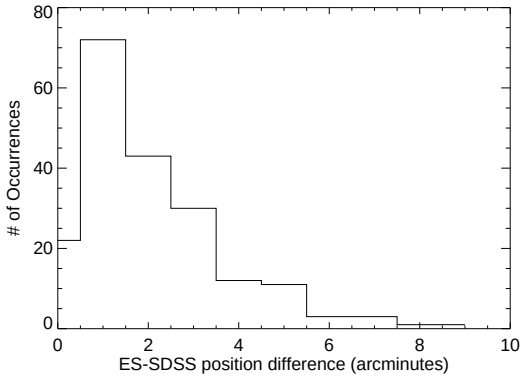

Figure 10. Distribution in positional differences between the radio and optical sources for the final list of 195 sources.

Column (7).– Velocity line width, W_{20}, measured at 20% level of the peak flux.

Column (8).– Distance, D, in Mpc (see text for description).

Column (9).– The logarithm of the HI mass, M_{HI}, calculated using equation (3) in units of solar masses.

3 OPTICAL IDENTIFICATION AND OBSERVATIONS

We determined that the best source of optical data to follow up the radio survey would be the SDSS. With its 5 photometric bands (u, g, r, i, z), it offers a unique and homogeneous data-base. The SDSS was however initially aimed at working on small faint objects and the pipeline software was not designed to cope with the arcminute sized galaxies which turn up in the ES so that up to now most SDSS galaxy work has had to be confined to objects beyond z = 0.02 (e.g. Blanton et al. 2003). Identifying the various large galaxy problems, finding and validating solutions for them, and rewriting parts of the software has held up the ES for at least 2 years. This is no place to discuss those corrections as an account appears in West et al. (2008). We summarise them only briefly to emphasise how necessary they are when using SDSS to study galaxies of arcminute size.

3.1 Limiting surface brightness

One legitimate concern about the SDSS, which is a relatively shallow survey ($\sim$ 55 s exposure per point), is whether it will go deep enough to detect the kind of LSBGs one might hope to find in the ES. Tests show that the main source of noise in looking for dim extended objects in the SDSS is photon noise in the sky subtraction (West et al. 2008, Strateva et al. 2001). In that case it can be shown that:

$$f(a) \geqslant \left(\frac{S}{N}\right) \frac{1}{\theta''} \frac{1}{\sqrt{N(a)}} \tag{7}$$

where f(a) is the fraction of the sky level one can go down to and find objects of angular size θ'' (diameter in arcsec) with a given signal-to-noise f(a) is that fraction for filter a, while N(a) is the total number of photons accumulated from the sky arcsec^{-2} through filter a. For the g-band SDSS N(g) $\sim$ 120, and if one demands a S/N of at least 10 for detection:

$$\overline{\mu}_{21}(g) \leqslant 22.1 + 2.5\, log_{10}\, \theta'' \tag{8}$$

For mapped galaxies the θ''_{21} is typically 10 θ''_{50} where θ''_{50} is the half light radius (e.g. Salpeter & Hoffman 1996). As $\overline{\mu}_{21}$ = μ_0 + 3.84, detection with SDSS in the g band requires:

$$\mu_0(g) \leqslant 20.8 + 2.5\, log_{10}\, (\theta''_{50}) \tag{9}$$

In contrast LSBGs are generally defined to have $\mu_0(B) < 23.0$ (see below). In other words, as you would expect of such a short exposure survey, the SDSS will be capable of picking up LSBGs only if they have large angular size ($\theta_{50} > 10$ arcsec). In the case of the ES all the sources are nearby ($\leqslant$ 10,000 km s^{-1} away) and although some of our claimed identifications lie close to the SB detection limit (18), they appear visible because they have patches of light that are brighter than average, such as HII regions. Of course we will not detect galaxies with relatively small fractions of HI, dEs and dSphs for instance, unless the galaxies are very massive. We can quantify this limitation by combining (9) with (5) in which case, for typical values of log $N_{HI} \sim 20.5$ cm^{-2} (Minchin et al. 2003) and sky brightness, μ_{sky}(g) = 22.5 g mag arcsec^{-2}, the ES will only detect galaxies for which:

$$\theta''(g)/(M_{HI}/L_B)_\odot \geqslant 15'' \tag{10}$$

where θ'' is the optical diameter (corresponding to $2 \times \theta_{90}$) in the g band. Gas poor galaxies will only be found if they are close by (i.e. θ'' large). In other words the ES may miss a significant fraction of light in the Universe coming from gas-poor galaxies. It is no coincidence that all the galaxies we do detect appear to be late-type.

Many definitions of galaxy SB, and what constitutes low SB, appear in the literature. For instance there are two quite different definitions of effective SB that are current: μ_{50}, which is the actual SB at the half-light radius, and $\overline{\mu}_{50}$ which is the mean value of the SB *within* the half-light radius. To avoid even further confusion we list all these definitions together in Table 3 and relate them all to the central SB μ_0. The relationships are only valid for pure exponential profiles. Where we have converted from SDSS colors to B-V system we have used Cross et al. (2004).

What constitutes a low surface brightness galaxy must be a matter of convention. However most optically selected surveys show a distribution in SB, however defined, which is approximately Gaussian with a FWHM $\sim$ 3.0 magnitudes. Thus galaxies with a SB 1.5 or more magnitudes dimmer than the peak value could reasonably be defined as LSBG's and that seems to be a common, though not universal, convention (e.g. Impey & Bothun 1997). For photographic, and for shallow CCD surveys, the peak in

Table 3. Definitions of surface brightness for galaxies with pure exponential profiles

Surface Brightness measurement	**Definition**
μ_0	Central Surface Brightness (SB)
μ_{50} (= μ_0 + 1.82^m)	The SB *at* the half-light radius (sometimes called 'effective SB')
$\overline{\mu}_{50}$ (= μ_0 + 1.12^m)	The mean SB *within* the half-light radius (also called 'effective SB')
μ_{90} (= μ_0 + 3.9^m)	The SB *at* the 90-per-cent-light radius
$\overline{\mu}_{90}$ (= μ_0 + 2.3^m)	The mean SB *within* the 90-per-cent-light radius
$\overline{\mu}_{21}$ (= μ_0 + 3.84^m)	The mean SB *within* the outermost 21-cm contour (see text)

NOTE.– μ_0 in magnitudes corresponds to the central SB I_0 where $I(r) = I_0 e^{-r/\alpha}$ and α is the scale length. Their total luminosity $L_T = 2\pi I_0 \alpha^2$; R_{50} = 1.68 α, R_{90} = 2.32 R_{50} and (empirically) $R_{21} \approx 5\ R_{50} = 8.4\ \alpha$.

the disc SB distribution appears to lie close to the Freeman value of μ_0(B) = 21.65. Thus any disc dimmer than μ_0(B) = 23.0 μ(B) could reasonably be regarded as LSB. The median SB for the ES, allowing for average bulge-to-disk ratio of $\sim$ 0.1, is $\mu_0(B) \sim 22.5$ mag arcsec^2, or about 0.8 mag arcsec^2 dimmer than the Freeman value for optical surveys, and we find objects as dim as $\mu_0(B) \sim$ 24 mag arcsec^2.

3.2 Identification of optical counterparts

The unambiguous identification of optical counterparts to 21-cm sources found in a blind survey like ours is by no means trivial. Because of the strong clustering of galaxies, both in angular and in redshift space, it is all too easy to find a plausible optical counterpart for virtually every 21-cm source. It is surprising, for instance, that in HOPCAT, the published optical catalogue for the 4315 HIPASS sources in the Southern sky (Doyle et al. 2005) there is not one source, not one intergalactic gas cloud or dark galaxy without a plausible optical counterpart. We shall now estimate the rate of false identification, i.e. the probability of finding a random optical galaxy within a given distance, in both angular and redshift space, of any given HI source. We shall assume, as the observations clearly suggest (Staveley-Smith et al. 1996) that optical galaxies and HI sources are clustered together. For an ES or HIPASS source the acceptable volume V_{acc} in which an optical counterpart could lie is a long thin cylinder, centred on the source, with its long axis, set by the radial-velocity uncertainties, along the line of sight. For an ES source at a typical radial velocity of 2000 km s^{-1}, the angular uncertainties in position (= R_0) (up to 5 arcmin) correspond to $\sim$ 50 kpc, while the velocity uncertainties ΔV, taking account of both radio and optical uncertainties, amount to $H_0\ \Delta V$ ($\sim$30 km s^{-1}) ($\equiv$ h) or half a Mpc. Given the correlation function:

$$p(r)dV = n_0 dV[1 + \xi(r)] \tag{11}$$

where $\xi(r) = \left(\frac{r}{r_0}\right)^{-1.8}$ and n_0 is the average number of plausible galaxies Mpc^{-3}, it is possible to integrate the probability of finding a random galaxy within the volume V_{acc} of the acceptable cylinder. To a very good approximation the number within a projected distance R_0 (in Mpc) of the source is given by

$$N(< R_0) \approx 1.8\ n_0\ r_0^{1.8}\ R_0^{1.2}\ (r_0 \approx 8Mpc) \tag{12}$$

Notice that the number is only weakly dependent on R_0 (because of the strong correlation) and dependent on the radial-velocity uncertainty not at all. This last is counter-intuitive but arises from the long thin shape of the cylinder. The ends of the cylinder are so very far from the centre that finding highly correlated galaxies within the ends is very unlikely. Conversely, obtaining very accurate optical velocities for plausible galaxies in the field does not greatly enhance ones chances of making an unambiguous identification when the HI velocity-uncertainties may still (for S/N reasons) be larger (and oddly enough, making blind HI surveys with bigger dishes will not help because the characteristic sources will be proportionately farther away (Disney 2008).

Table 4. Number of random galaxies within D (Mpc) $\Delta\theta$ (rad) of radio position.

R_0 (1)	N($< R_0$) (2)
2	78
1	35
0.5	13
0.3	8
0.2	5
0.1	2.1
0.07	1.3
0.05	0.8
0.03	0.4
0.01	0.1

To turn equation (12) into numbers it is necessary to adopt an optical Luminosity Function for the putative galaxies. If we adopt:

$$\varphi(M) = \varphi_* \kappa^{\alpha+1} e^{-\kappa} \tag{13}$$

where $\kappa \equiv 10^{0.4(M_*-M)}$, α = 1.2, φ_* = 2.1 $\times$ 10^{-2} h^{-3} and M_* = $-$20.04 $-$ 5 log h (Blanton et al. 2003) then Table 4 where Col. (1) gives the angular size distance in Mpc, $R_0 = D\ \Delta\theta$, D is the source distance in Mpc, $\Delta\theta$ is the angular distance between the source and the optical counterpart in radians and Col. (2) is the number of random galaxies (down to 3 mag below M_*) to be expected within that distance. As an example, consider a source at a typical radial-velocity-distance of 2000 km s^{-1} in ES ($\sim$ 27 Mpc) where 1 arcmin corresponds to $\sim$ 8 kpc. The typical positional uncertainty in HIPASS $\sim$ 1.3 arcmin (Meyer et al. 2004, Zwaan et al. 2004) corresponds to $\sim$ 0.01 Mpc. At that distance, according to Col. (2) of Table 4, there is a 10 per cent chance of finding a random galaxy of roughly the right radial velocity, i.e. clustered with the HI source, within the positional uncertainty. And the chance of a misidentification could be higher still if one was prepared to consider, as plausible candidates, objects more than 3 mag below L_* in the luminosity function (our assumption in table 3). Note that Doyle et al. (2005) identify optical candidates up to 5 arcmin away, leading to the probability of a plausible misidentification *at that distance* of more than 1.

To reduce these potentially serious misidentification problems in ES we threw out all (90 out of 310) sources which looked, on inspection of the SDSS-DR2 fields, to have more than 1 plausible op-

Table 5. Petrosian Photometry of the ES sample

ES Name	RA (J2000)	Decl. (J2000)	u	g	r	i	z	PetroR$_{50}$ ($''$)	PetroR$_{90}$ ($''$)
(1)	(2)	(3)	(4)	(5)	(6)	(7)	(8)	(9)	(10)
HIPEQ0014−00	00 14 36	-00 44 42	13.77 ± 0.04	13.13 ± 0.02	12.91 ± 0.02	12.82 ± 0.02	12.77 ± 0.03	21.4 ± 0.4	59.0 ± 0.8
HIPEQ0027−01a	00 27 47	-01 09 39	14.72 ± 0.04	14.09 ± 0.02	13.85 ± 0.02	13.79 ± 0.02	13.87 ± 0.04	21.4 ± 0.4	43.6 ± 0.8
HIPEQ0033−01	00 33 22	-01 07 01	15.65 ± 0.06	14.86 ± 0.02	14.58 ± 0.02	14.44 ± 0.02	14.40 ± 0.05	20.2 ± 0.4	45.9 ± 1.6
HIPEQ0043−00	00 43 31	-00 06 49	13.90 ± 0.03	12.95 ± 0.02	12.52 ± 0.02	12.31 ± 0.02	12.14 ± 0.03	13.9 ± 0.4	36.4 ± 0.4
HIPEQ0051−00	00 51 57	-00 28 25	15.42 ± 0.03	14.60 ± 0.02	14.23 ± 0.02	14.06 ± 0.02	13.99 ± 0.03	6.3 ± 0.4	17.4 ± 0.4
HIPEQ0058+00	00 58 50	00 37 46	14.90 ± 0.03	13.91 ± 0.02	13.43 ± 0.02	13.19 ± 0.02	13.07 ± 0.03	10.7 ± 0.4	23.0 ± 0.4

NOTE.– An extract of the table is shown here for guidance. It is presented in its entirety in the electronic edition of the Journal.

tical counterpart within the radio beam (FWHM $\sim$ 14 arcmin) and we obtained accurate optical velocities for all the rest using either those provided in NED, the SDSS-DR2 fibre or, for 20 galaxies, the Dual Imaging Spectrograph on the 3.5 metre telescope at Apache Point Observatory. All candidates with optical velocities discrepant from the HI value by more than half the 21-cm line-width ΔV_{20} were discarded. In addition, a number of other sources were removed either because they extended across 2 or more SDSS-DR2 fields, or because there was a saturated foreground star within 1 arcmin.

Altogether of the original 310 HIPASS sources with plausible SDSS-DR2 galaxies within the HIPASS beam and at the right redshift (as defined above) 90 were thrown out because of multiplicity i.e. for there being more than 1 (up to 5) good SDSS-DR2 candidates, 20 were too extended and 5 too near a bright star. Fig. 9 shows the distribution of velocity differences $\Delta V/W_{20}$ for the *original* 310 candidates and Fig. 10 shows the distribution in positional differences between the radio and optical sources for the 195 which remain in the final ES list. The tail in this plot is due to the HI centroid not being centered in the optical source.

Most of the identifications fall within 2 arcmin of the radio position, consistent with the errors in those positions measured in the general HIPASS catalogue using interferometry (Meyer et al. 2004). Nevertheless there remain a tail of optical candidates up to 7 arcmin (half the FWHM beam) away from the radio centroid. Because of clustering (see Table 3) we can not rule out the possibility that a handful of sources (probably less than 10) remain misidentified. This is too small a number to invalidate the main results. Nevertheless we should acknowledge biases in our sample against galaxies in tight groups (too many in the beam), galaxies that appear very large (overlapping SDSS-DR2 fields), and dark galaxies or intergalactic clouds for which we will too easily find plausible, optically bright alternatives. Most of these biases are difficult to avoid and must exist to an equal or greater extent in other HI selected blind samples. In particular the number of sources ($\sim$ 30 per cent) discarded because of clustering within the beam highlights the difficulty of measuring HI mass functions which are not somehow adjusted for confusion.

The data we used all came from SDSS Data Release 2 (Abazajian et al. 2004) using the pipeline from DR3 (Abazajian et al. 2005) but no SDSS catalogue data was used, for reasons outlined below. DR2 covers 3324 deg^2, about half of which overlaps the ES. SDSS pipeline photometry of large galaxies is very inaccurate for a number of reasons. The pipeline shreds large galaxies into a number of pieces, circular apertures are not appropriate, the inclination is not properly taken account of and worst of all sky subtraction can subtract much of a large galaxy away from itself. Thus we had to find ways of measuring the significance of all these problems and devise alternative methods of handling the data. These are discussed at length in West (West PhD thesis) and are being published (West et al. 2008) so that the community wanting to use SDSS to work on nearby galaxies can make use of them.

Table 5 lists the SDSS-DR2 optical data for the ES sample.

Column (1).– ES source name.

Columns (2) and (3).– Right ascension and declination (J2000) of the optical position of each SDSS-DR2 source.

Columns (4) to (8).– Petrosian magnitudes in each SDSS band u, g, r, i, z, Unlike the native SDSS-DR2 Petrosian magnitudes, our Petrosian apertures are elliptical. The shape of each aperture is defined from two-dimensional Sersic fits and we use the g-band to measure both the shape and size of each Petrosian aperture. For some galaxies in the sample, a Sersic profile was not a good fit. In these cases, a circular aperture was used.

Columns (9) and (10).– The PetroR50 and PetroR90 values reported are the g-band semi-major axes that encompass 50 per cent and 90 per cent of the total Petrosian flux respectively. All of the SDSS data are described in West et al. (2008).

4 THE DIVERSITY OF SOURCES

In this section, we show just how diverse the galaxies in a blind HI survey actually are. A quick way to grasp the wide diversity of types within the ES is to examine their SDSS-DR2 images, which can be seen online (http://www.astro.washington.edu/HIgalaxies) showing a g, r, i composite image. They range between red, early type barred spirals several times more luminous than L$_*$, containing proportionally small amounts of gas [(M$_{HI}$/L$_B$) < 0.2], and extremely low surface brightness objects hundreds of times fainter, very blue, consisting almost entirely of gas and so irregular in optical appearance as to be 'Inchoate', i.e. to be made of nothing more than irregular smudges with apparently unconnected higher surface brightness patches here and there. Given just how difficult such Inchoates are to see at all on the SDSS-DR2 it is perhaps surprising that not a single source lacks an optical counterpart - however ragged it may be. There is even one elliptical galaxy, HIPEQ0154−00, which appears to have a thin disc and it is being investigated further.

To consider the diversity of sources in more detail we consider four individual galaxies each representing a different characteristic 'class-type' of object that is quite common in the sample. As a fiducial comparison one can pick say HIPEQ1507+01 (NGC5850) which is typical of the kind of galaxy that turned up in optically selected catalogues and which were afterwards examined at 21-cm (e.g. Huchtmeier 1988). It is optically very luminous,

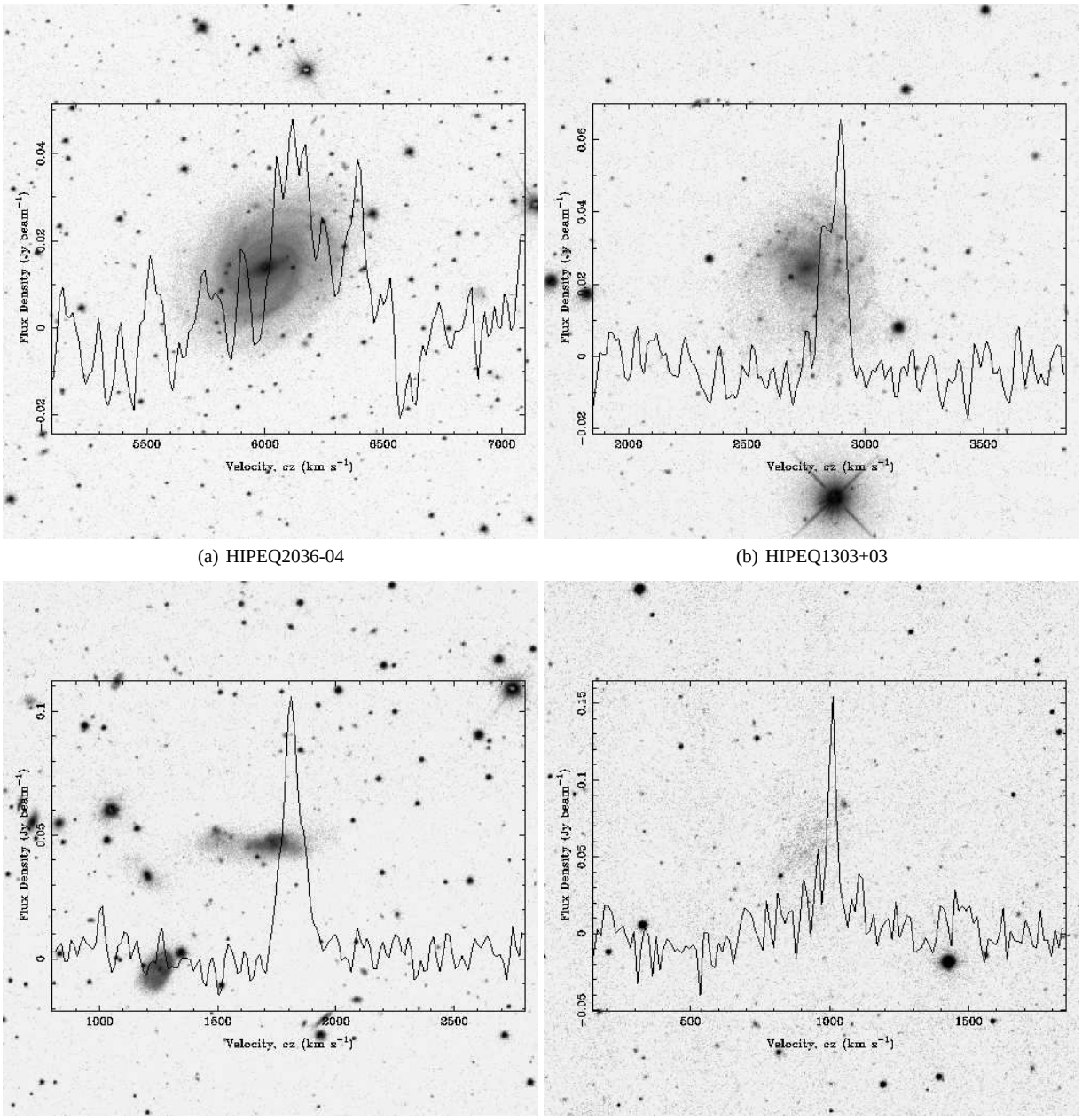

(a) HIPEQ2036-04 (b) HIPEQ1303+03

(c) HIPEQ0821-00 (d) HIPEQ1145+02

Figure 12. These images illustrate characteristic galaxy types within a blind HI survey such as the ES, with their HI spectra superposed. (a) shows a 'Hydrogen Giant'; (b) a massive LSBG; (c) an Irregular Galaxy and (d) an 'Inchoate Galaxy' - see text.

1.7^m brighter than L_*, has a low M_{HI}/L_B = 0.15 but nevertheless contains a significant amount of HI (log M_{HI} = 9.8) simply because of its high luminosity. It is early type (T=3), red [$(g-r)$ = 0.63] and dynamically very massive (log M_{dyn} = 11.7 $M_\odot$) where $M_{dyn} = R_{50}(g) \times (W_{20}/sin(i))^2/G$.

The greatest number of galaxies in the ES are late type spirals a magnitude or so fainter than L_* but gas-rich (i.e. median M_{HI}/L_B = 0.91 $\pm$ 0.16) and blue.

(i) Our first 'HI Selected' type is a *'Hydrogen Giant'*, that is to say a galaxy with more than 10^{10} $M_\odot$ of HI. HIPEQ2036−04 (NGC6941) contains 2 $\times$ 10^{10} $M_\odot$, apparently an upper limit if one excludes other nearby companions - as here, and about 5 times the HI mass of the Milky Way (Binney & Merrifield 1998) [Fig 12(a)]. Their huge hydrogen content means that such galaxies can be detected far away and this one is at 6200 km s^{-1}. It is also a giant optically, being $\sim$ 3 L_* in g but its gas-to-light ratio is M_{HI}/L_B = 0.7 that is 5 times higher than the fiducial value for giants. Fig. 12(a) shows an SABb (T=3) with a high surface brightness core but a low surface-brightness disc with widely spread spiral arms. The integrated colour is $(g-r)$ = 0.79, while the fibre spectrum of the core is typical of an early type spiral. What is remarkable about these Hydrogen Giants is that they appear to have slowed their star-formation and so still contain as much mass in gas as in stars. The dynamical mass is high (log M_{dyn} = 11.3), but 1.5 times less than NGC5850, the fiducial galaxy. There are 20 in the survey, but given their generally high redshifts (median $\sim$ 5500 km s^{-1}) hydrogen

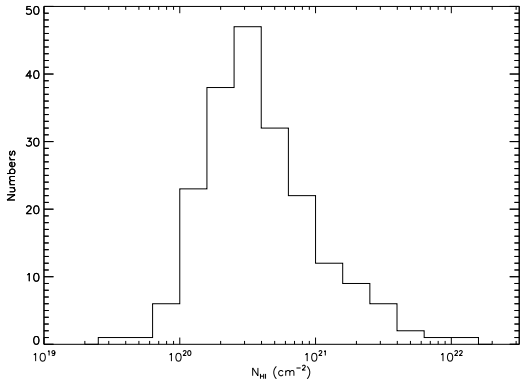

(a) Distribution of column densities

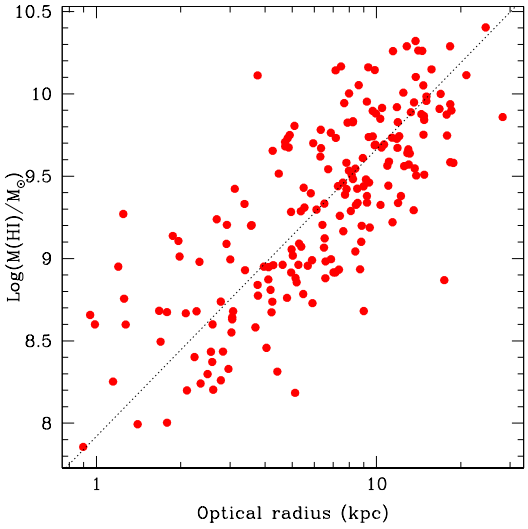

(b) The HI mass/radius correlation

Figure 11. (a) shows the Distribution of column densities for the ES sample where the densities are obtained by assuming $\theta_{21} = 5 \times \theta_{50}\ (opt)$ - see text. (b) shows the HI-mass/radius correlation, i.e. constant column density. The dotted line shows the best linear fit to our data.

giants cannot be common in space. The astrophysical challenge is to explain their delayed evolution from gas into stars.

(ii) Our second class-type is the low surface brightness galaxy of the more massive kind - typically an anaemic spiral like HIPEQ1303+03 (UGC08153) shown in Fig. 12(b) (other good examples are HIPEQ1228+02 and 2337+00). It truly is low SB with a $\overline{\mu}_{50}(g)$ = 24.3 and yet its dynamical mass is $10^{10.9}$ $M_\odot$. Formally speaking there are even more massive LSBGs in the sample but their discs are so extremely dim that estimating an accurate axis-ratio, necessary to calculate a dynamical mass, often becomes problematic. The total luminosity is 0.5 L_* [M_g = -18.8] and the Hydrogen content is $\log_{10}$ M_{HI} = 9.0 [M_{HI}/L_B = 0.77]. The colour is blue, (g − r) = 0.27, as is commonly the case with LSBGs (McGaugh et al. 1994) but there are also some reddish ones in the survey. The question of how significant LSBGs are in cosmic terms (e.g. Fukugita et al. 1998) hinges upon two difficult questions: on how massive they are and how common. HIPEQ1303+03 and its like confirm, beyond question, that true LSBGs can be massive (see also Sprayberry et al. 1993). To what extent blind HI surveys can compensate for the dramatic selection effects against LSBGs in optical catalogues is not yet clear. Certainly such surveys find healthy numbers of LSBGs. However Fig. 13 shows that although N_{HI} is more or less constant in the sample, there is a perceptible fall-off in the column density with SB, with a sharp cut-off at $10^{19.7}$ HI atoms cm^{-2}. This is due to the instrumental limit of the Multibeam system for 400 sec integration so it could still be missing some low SB objects (see Minchin et al. 2004). There are $\sim$ 10 LSBGs with dynamical masses $> 10^{10}$ $M_\odot$, and as many again which are just as dim apart from a small bright core.

(iii) Our third type is the irregular for which HIPEQ0821−00 (UGC04358) in Fig. 12(c) serves as an example though they are very heterogeneous. ES irregulars are naturally gas-rich, HIPEQ0821−00 having (log M_{HI} = 9.3) almost as much HI as the Milky Way with an M_{HI}/L_B = 3.3. At M_g = − 16.4 it is $\sim L_*/20$, has a very blue colour [(g − r) = 0.17] and moderately high SB ($\overline{\mu}_{50}(g)$ = 22.5) though SB's among the type vary by 5 magnitudes and global SB's for such irregular objects are rather meaningless. There are at least 30 irregulars in the ES sample.

(iv) The last 'type', the 'Inchoates', are so dim and faint that they could scarcely be found in any other but a blind HI survey. Our example HIPEQ1145+02 [Fig. 12(d)] can barely be seen on the SDSS, having a SB $\overline{\mu}_{50}(g)$ = 24.8 at the very limit of the survey. We detect it only because it has a lot of hydrogen for its luminosity (M_{HI}/L_B = 7) which at M_g = −14.31 is 1/200 L_*. The 'Inchoate' label for these objects derives from their apparent total lack of organisation. More irregular than irregulars, they have no cores or obvious centres, and appear as merely haphazard enhancements of SB at what appear to be HII regions. In addition to being extremely gas-rich ($M_{HI}/L_B > 5$) they are generally blue, thus HIPEQ1145+02, by no means extreme in colour, has B − V = 0.48 and (g − r) = 0.27. Other good examples of what is a virtually new type of galaxy are HIPEQ0238+00, 0240+01, 0958+01, 1227+01 and 1256+03. We say 'virtually' because one of them, HIPEQ1227+01, is the famous cloud serendipitously found by Giovanelli and Haynes (1989) and at first thought to be a protogalaxy. Indeed it would have been the easiest Inchoate to find as it has the highest M_{HI}/L_B ($\sim$ 22) of *any* object in the ES sample.

Now that we have a dozen or so 'Inchoates' in the ES to study, some of the puzzling questions raised by the original Giovanelli and Haynes cloud return with even greater insistence. It is the *combination* of their properties which makes it difficult to explain Inchoates (Salzer et al. 1991, Grossi et al. 2007). Their extraordinarily high gas-mass fraction indicates little integrated past star formation, while their blue colours [as blue as (B−V) $\leqslant$ 0.3] can only be explained with star formation that rises sharply to the present day (Bruzual and Charlot 2003). However, if such a rise is only a temporary burst, then the galaxies should soon fade by 1.5 magnitudes while reddening from (B−V) = 0.3 to 0.5, leaving behind an optically undetectable dark HI cloud (Leitherer et al. 1999). However there are no such dark clouds in our survey, and none among 4315 HIPASS sources detected across half the sky (Doyle et al. 2005), all of which are optically detected in either SDSS or the SuperCosmos Sky Survey (Hambly et al. 2001). Thus a bursting explanation for their blue colours seems less likely than either a truly young galaxy or a steadily rising star formation rate. However, GALEX measurements of 2 of them (1145+02 and 1256+03) imply current star formation rates that are only a factor of $\sim$ 2 greater than the past average. And if they were truly young, why do not blind HI surveys like HIPASS find their predecessor dark protoclouds? 'Inchoates' are indeed a puzzle.

Whatever they are, Inchoates make a dramatic contrast with fiducial galaxies like NGC5850 and with the higher SB spirals

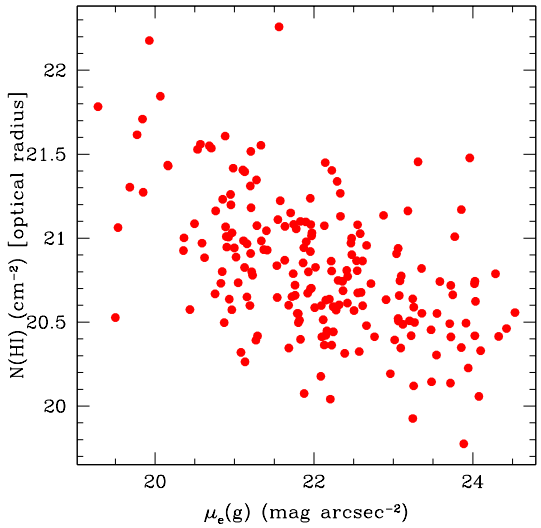

Figure 13. The surface brightness/column density correlation for the ES galaxies where SB=$\overline{\mu}_{50}(g)$, see Table 3.

which make up more than half the sources in the ES sample. Together with luminous gas-poor galaxies, hydrogen giants, massive LSBGs and irregulars they illustrate a diversity which suggests a wide scatter among several underlying fundamental parameters such as mass, age, angular momentum and binding energy. But such turns out not to be the case.

5 CORRELATIONS AMONG GALAXY PROPERTIES

We have measured 9 quantities in all, combined with the inclination (b/a) which can be used to correct observed quantities to face on: mass of HI, HI line width (as defined in Section 2), luminosity (in g), four colours $(u-g)$, $(g-r)$, $(r-i)$, and $(i-z)$, and 2 radii (R_{50} and R_{90} in g band) all defined in Section 3. What we are chiefly missing is some kind of environmental parameter, which could be vital. However we have been so fastidious in excluding closely packed galaxies that we cannot use environment for now. Later, with more interferometry of the dubious identifications within groups, we can add that to the study. Even so it is worth pressing ahead without it, provided we remember the caveat, because Gavazzi et al. (1996) showed that for the late type galaxies which appear in the ES, environment appears to be unimportant.

From the 9 basic measurements, and the inclination and assumed distance, one can construct other more familiar and perhaps more interesting parameters such as circular velocity (V_0), dynamical mass M_{dyn} ($\sim V_0^2 R_{50}/G$), surface brightness $\overline{\mu}_{50}(g)$ ($\sim L_g/R_{50}^2$), column density ($N_{HI} \sim M(HI)/R_{90}^2$), brightness temperature T_{HI} ($\sim N_{HI}/\Delta W_{20}$), angular momentum per unit mass ($q \sim V_0 R_{90}$) and so on. With at least 15 such synthetic parameters to work with there are $\approx (15\times14/2) \approx 100$ correlations to look for. We could have used some statistical technique but we elected to look at all the correlations by eye for now. Correlation coefficients, and their significance are given for each correlation. Thus one can discount obvious selection effects, and the already well-known correlations, to concentrate on looking for what might be new or surprising.

We are of course far from the first to attempt such a systematic search among galaxy properties. For instance Brosche (1973), Balkowski (1973), Tully & Fisher (1981), Gavazzi et al. (1996),

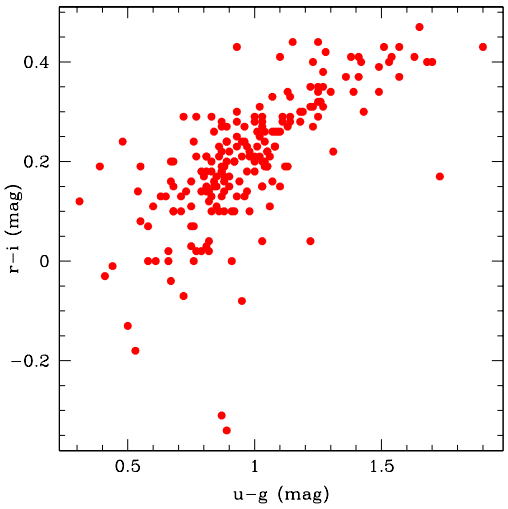

(a) $(r-i)$ vs $(u-g)$ relation

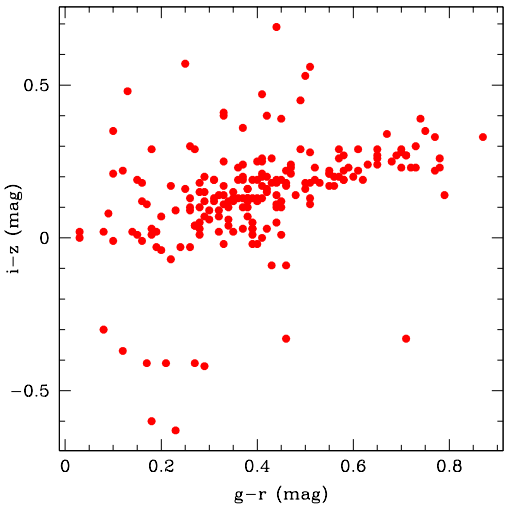

(b) $(i-z)$ vs $(g-r)$ relation

Figure 14. (a) shows the relations between the $(u-g)$ and $(r-i)$ optical colours and (b) shows the relation between the $(g-r)$ and $(i-z)$ optical colours of the ES sample.

Blanton et al. (2003) looked at optically selected samples but with added HI data, whilst Minchin et al. (2003), Rosenberg et al. (2005), Kovac (2007) and Begum et al. (2006) have recently looked at HI selected sets followed up either by optical or by NIR measurements from 2MASS. Elsewhere we shall compare results, but for now we examine only our own correlations with an eye unbiased by previous work.

As a start it is important, given the rather small number in the sample (195), to establish that there is sufficient dynamic-range within its intrinsic properties to make correlation analyses worthwhile. To look for relations between two galaxy properties *y* and *x*, of the form $y = Ax^m$, it is elementary to show that the error on *m* due to measurement errors δy, δx, as opposed to real scatter in the properties themselves, is given by:

$$\sqrt{\left\langle \frac{\delta m}{m} \right\rangle^2} \approx 1.5 \sqrt{\left(\frac{(\delta y/y)}{\Delta(magy)} \right)^2 + \left(\frac{(\delta x/x)}{\Delta(magx)} \right)^2} \qquad (14)$$

Table 6. Properties of the ES sample with optical SDSS-DR2 data.

Property (1)	Median (2)	Min (3)	Max (4)	Range (5)	Relative error (6)
Mass HI ($M_\odot$)	$10^{9.38\pm0.40}$	$10^{7.5}$	$10^{10.2}$	6.8	.03
Luminosity (g) ($L_\odot$)	$10^{9.51\pm0.38}$	$10^{7.2}$	$10^{10.6}$	8.5	.01
Area (πR_{50}^2) (kpc^2)	$10^{1.91\pm0.1}$	$10^{-0.2}$	$10^{3.12}$	8.3	.01
Line-width W_{20} (km s^{-1})	$10^{2.12\pm1.78}$	$10^{1.60}$	$10^{2.60}$	2.5	.09
Surface brightness ($L_\odot pc^{-2}$)	$10^{1.85\pm0.07}$	$10^{0.88}$	$10^{2.99}$	5.2	.01
Dynamical mass ($M_\odot$)	$10^{10.14\pm0.53}$	$10^{8.5}$	$10^{11.3}$	7.0	.06
Colour ($g-r$)	0.39 ± 0.11	0.1	0.7	0.6	.07

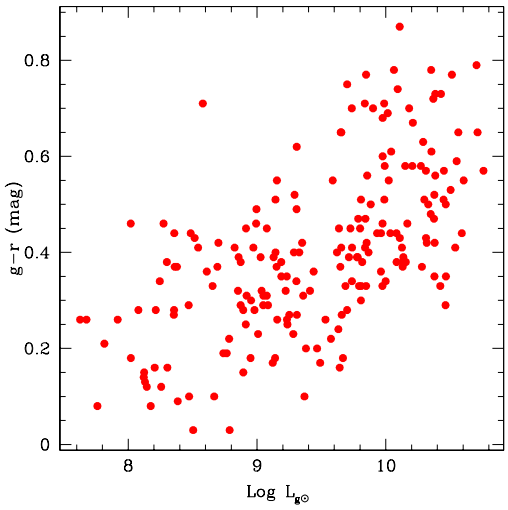

Figure 15. The $(g-r)$ colour/luminosity relation.

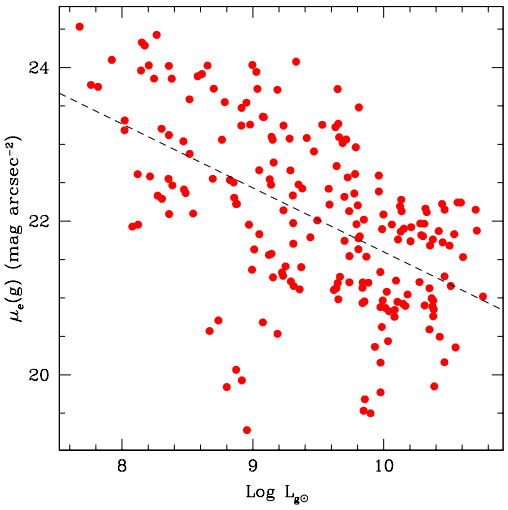

Figure 16. The surface brightness/luminosity relation in g band. The dotted line shows the best linear fit to the data.

where $magx \equiv 2.5\ log_{10}(x)$ and the $\Delta(mag)$'s give the relevant dynamic ranges. Table 6 shows in *Column (1)* the most relevant properties measured for the galaxies in the ES sample.

Column (2).– Median value of the measurement.

Columns (3) and (4).– The maxima and minima values respectively, where the few objects in the extreme wings of the distribution have been ignored.

Column (5).– Dynamic range in magnitudes.

Column (6).– Shows the estimated relative measurement errors, $1.5(\delta x/x)/\Delta(mag\ x)$.

In most cases the relevant measurement errors are small enough ($<$ 0.1) not to dominate a correlation with another quantity in the table, the main exceptions being line-width W_{20} and colour. We do not use line-width except in the combination $W_{20}^2 R/G$, i.e. dynamical mass, where the relative measurement errors are reduced by the large dynamic range to < 0.06.

First notice that the 4 colours are strongly correlated (Fig. 14), as was to be expected, so there is considerably degeneracy among them and, as revealed already, to first order there is only 1 independent colour (Strateva et al. 2001). Many properties correlate with luminosity and Fig. 15 shows the colour-luminosity diagram, which is well known for optically selected galaxies, i.e. more luminous galaxies are redder. When it comes to disentangling the physics going on the actual slopes in all such correlation diagrams will be crucial. Thus Fig. 15 implies that $L_r \sim L_g^{1.1}$ roughly. The Pearson correlation coefficient is $r_p \sim 0.61$, corresponding to a probability $P(r > r_p) > 99.9\%$. This is the first of the 5 correlations.

Fig. 16 exhibits the second correlation ($r_p \sim -0.55$, $P(r > r_p) > 99.9\%$), i.e. between surface-brightness and luminosity and, not unexpectedly less luminous galaxies are dimmer. While this has been long suspected (e.g. Bingelli 1984) one could never be certain, in any optically selected sample, to what extent it was an artefact of the dramatic selection effects acting on surface-brightnesses which lie so close to the sky (e.g. Disney 1999). However here all the galaxies have been identified without regard to their optical properties and it seems very likely that Fig. 16 tells us something fundamental about the relation between luminosity and radius with few selection effects. While the scatter is large the correlation is clear and very roughly speaking the surface brightness $\Sigma(g) \sim L_g^{0.5}$.

The third correlation ($r_p \sim 0.75$, $P(r > r_p) > 99.9\%$), between HI mass and optical radius, is illustrated in Fig. 11. It is a tight one and suggest, that all galaxies have the same HI column density, i.e. $M_{HI} \propto R_g^2$. This was discovered first by Haynes and Giovanelli (1984) in an optically selected sample, discovered again in an HI selected sample by Minchin et al. (2003) and confirmed in an interferometer study by Rosenberg et al. (2005) in the Arecibo Dual Beam Survey and Kovac (2007) and our ES measurements concurs. For now constant surface density, is an intriguing puzzle which needs to be explained.

The fourth correlation ($r_p \sim 0.81$, $P(r > r_p) > 99.9\%$) we find is between luminosity (g) and dynamical mass shown in Fig. 17. Over more than 3 orders of magnitude the g luminosity is tightly correlated with dynamical mass, a correlation that appears percep-

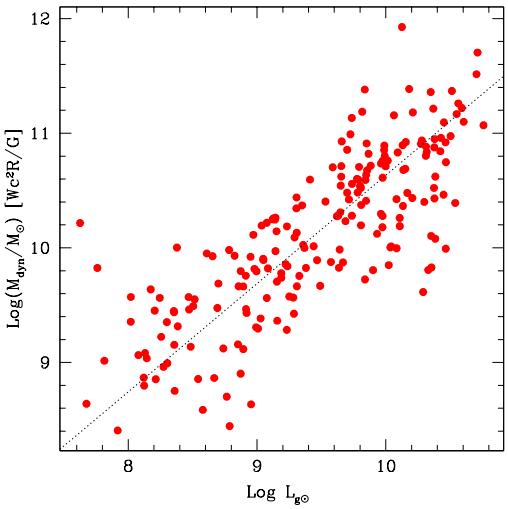

Figure 17. The dynamical mass/luminosity relation in g band. The dotted line shows the best linear fit to the data.

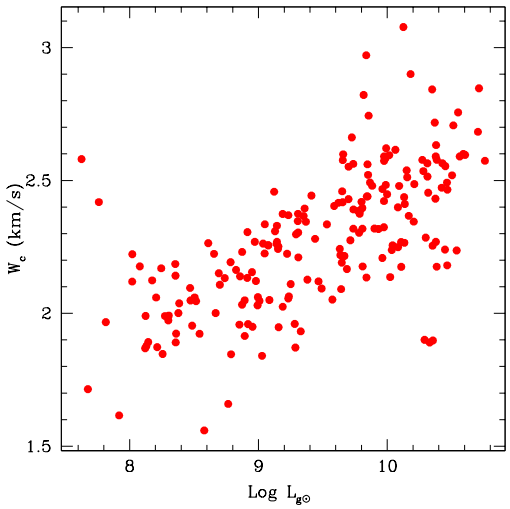

Figure 18. The Tully-Fisher relation in g band.

tibly tighter than the Tully-Fisher correlation which we show in Fig. 18 (see later). The slope is close to 1, implying a direct proportion between dynamical mass and luminosity. This is not new either but it was discovered in the remarkable paper by Gavazzi et al. in 1996. In order to compare our data with Gavazzi's, we transform ours into the H-band, which should be freer of dust and of transient star-formation effects. 113 of our ES sources are in 2MASS and Fig. 19 illustrates the relation between their colour and their luminosity, which implies:

$$\log(L_H) = (1.31 \pm 0.05) \times log(L_g) - (2.9 \pm 0.4) \qquad (15)$$

i.e. $L_H \sim L_g^{4/3}$. If we use this to transform our Fig. 17 data into the H-band we reach Fig. 20 where our galaxies are plotted on top of the GOLDMine sample assembled by Gavazzi and colleagues (2003) for a mixture of bright discs and Virgo dwarfs. Over almost 4 orders of magnitude, disc-like galaxies have $M_{dyn} \sim L_H$ with a scatter of only $\sim$ 1 mag about the relation in both axis directions. Whether they are selected optically (Gavazzi), or by their neutral hydrogen signal as here, the 635 galaxies all appear to have the same H-band Mass-to-Light Ratio $\sim$ 4 in solar units. The numerical value 4 is an artefact of using $R_{50}(g)$ in the conventional definition of M_{dyn}, which we have so far adopted. However $M_{dyn} \propto R \times (W_{20} sin(i))^2$ and as the outermost HI test particles are typically at $\sim$ 5 $R_{50}(g)$ in images 21-cm galaxies (Salpeter & Hoffman 1996, Kovac 2007) a more accurate M_{dyn} would be $\sim$ 5 times greater than we and Gavazzi have implied. In that case the H-band mass-to-light ratio for both our sample, and the GOLDMine sample, is $\sim$ 20, leaving plenty of scope for dark matter. Note that this ratio cannot be luminosity dependent (see Fig. 20). 'Gavazzi's relation' as we call it, is a remarkably uniform one for any extragalactic data-set.

The fifth and last correlation ($r_p \sim 0.18$, $P(r > r_p) \sim 99.9\%$) we look at in Fig. 22 is that between the two separate radii measured by SDSS i.e, R_{50} and R_{90}. The very tight correlation, and the ratio between them of 2.3 means that despite the very wide range of galaxy types in the ES their outer light profiles are all well fitted by an exponential law and the ratio does not change with luminosity.

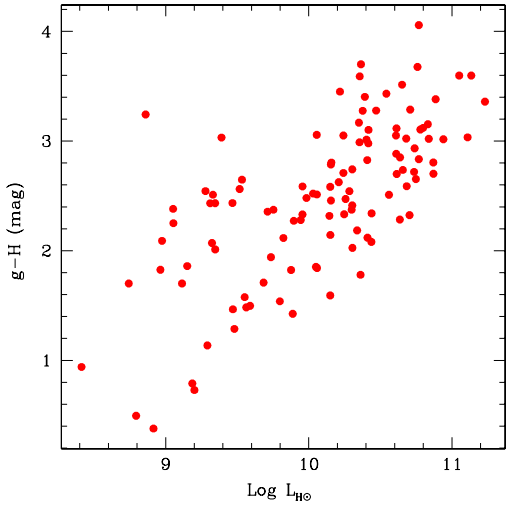

Figure 19. The $(g-H)$ colour H band luminosity relation for the ES galaxies detected by 2MASS.

6 DISCUSSION

We set out to look for correlations within a sample of galaxies free of optical selection effects. Apart from inclination and velocity we measured 9 parameters for each galaxy. Since the 4 colours appear degenerate we are left with 6 *a priori* independent observables, between which we find the following 5 correlations, 4 old and 1 new (A) which are shown in Table 7, where the columns are as follows.

Column (1).– Correlations observed.

Columns (2) and (3).– Denote the distance dependance, d^x, of the left and right-handed parameters in the correlation.

Column (4).– Indicates the difference between the two exponents in Cols. (2) and (3) (see text for explanation).

Column (5).– Shows the *observables* introduced into the correlation, that have not been used before.

Column (5) in Table 7 is pertinent to the *independence* of the 5 correlations. Unless *a priori* reasons can be advanced for a dependance of the new observables on previous ones, then the 5

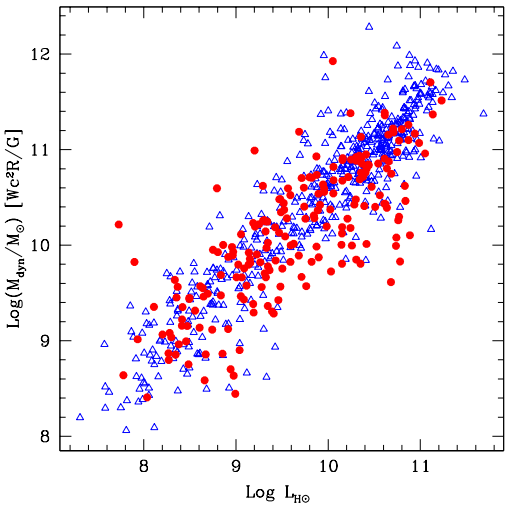

Figure 20. The dynamical mass-H band luminosity relation for our samples (circles) and for the GOLDMine sample (triangles).

Table 7. Correlations in the ES sample.

	(1)	(2)	(3)	(4)	(5)
A	SB/Lum	d^0	d^2	2	SB, θ_{90}, d
B	Col/Lum	d^0	d^2	2	$(g-r)$
C	M_{dyn}/L_H	d^1	d^2	1	ΔV
D	R_{90}/R_{50}	d^1	d^1	0	θ_{50}
E	M_{HI}/R_{90}^2	d^2	d^2	0	S (21cm)

correlations must be independent. It might, for instance, be argued that θ_{50} should depend on θ_{90}, but that ignores the real differences in 'concentration' q $\equiv \theta_{90}/\theta_{50}$ between galaxies of different morphological type (e.g. q = 2.3 for pure exponential but q = 4.2 for de Vaucouleur profiles). Concentration is a crude but quantitative proxy for morphological type, and there is no *a priori* case for this to be the same among HI-sources. Thus we can argue that the 5 correlations are truly independent.

Although the number of galaxies is modest the dynamic range of most of their properties is large (i.e. more than 7 magnitudes in luminosity, area, M_{HI} and M_{dyn}) whilst the correlations are, in a statistical sense, highly significant. So far as the *existence* of the correlations (our main interest here) is concerned the sample-size is not an embarrassment, though larger samples will be needed to pin down the *slopes* of the correlations more precisely. There is moreover a great diversity of galaxy types in the sample, ranging between early-type giant spirals and tiny 'Inchoates' of such low surface brightness that they would usually be, and indeed were, missed in optical surveys. The difficulty of making a reliable census of galaxies in light alone is illustrated by Fig. 16 where it can be seen that at all luminosities galaxies can vary in SB over 3 or 4 magnitudes, making the dimmest of them, even the giants, hard to pick out from the background by optical means alone. The narrow SB range of earlier catalogues (Freeman 1970, Disney 1976) was almost certainly a selection artefact.

Two correlations in particular need explaining. Correlation (E), i.e. $M_{HI} \sim R_g^2$ could be related to the stability of a gas layer to gravitational collapse, and hence to a trigger for star formation (e.g. Kennicutt 1989, Schaye 2008). The other, the SB/Luminosity

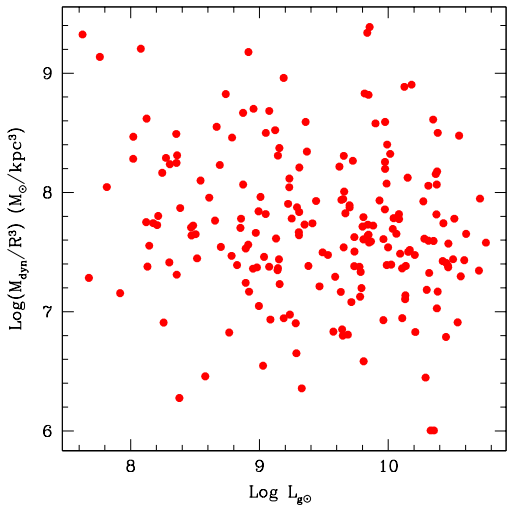

(a)

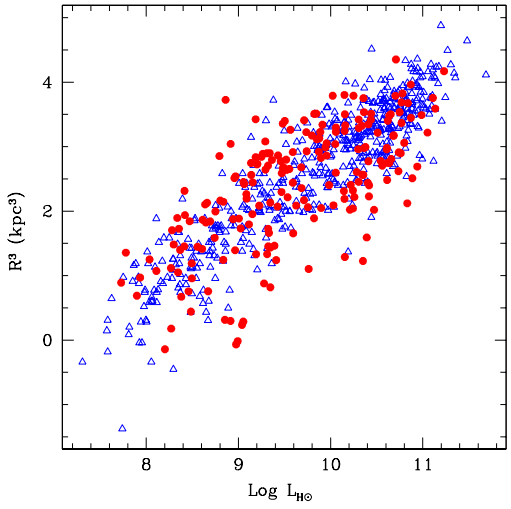

(b)

Figure 21. Top: The ratio M_{dyn}/R^3 ratio as a function of the g band luminosity. Bottom: The relation between the dynamical mass and R^3 for our sample (circles) and for the GOLDMine sample (triangles).

correlation (A) has considerable scatter (Fig. 16) making it difficult to pin down an accurate value for β in $\Sigma \sim L^\beta$, where β is not far from 1/2. Combining our data with the GOLDmine sample, in order to increase sample-size and hopefully reduce scatter, yields $\Sigma \sim L^{1/3}$, or $\Sigma \sim R$, or L_H/R_g^3 = constant or, considering Gavazzi's Law, M_{dyn}/R_g^3 = constant ($\sim$ 1 H atom cm^{-3} within the optical radius) which, see Fig. 21(b), is a pretty good fit. So the mass - and luminosity - density of galaxies is more or less independent of their Luminosity. This is at least a better mnemonic for recalling the rather scattered SB/Lum law. If true the Virial Theorem implies that all HI galaxies spin at the same angular velocity and rotate $\sim$ 40 times in a Hubble epoch.

What about the Tully-Fisher correlation $\Delta V \sim L^\alpha$? Gavazzi's Law (C): $L_H \sim M_{dyn} \equiv R_g \Delta V^2$ while above: $R_g \sim L_H^{1/3}$, hence $\Delta V \sim L_H^{1/3}$. In other words our data are consistent with the TF law provided α = 1/3 [see also Fig. 18]. The problem with using TF directly is demonstrated in Table 6 where it can be

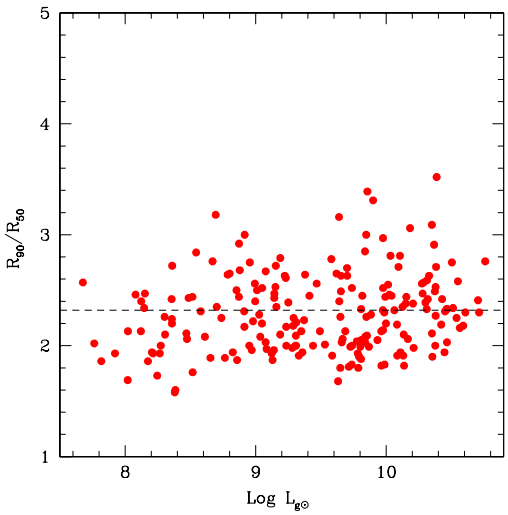

Figure 22. The concentration index of HI galaxies as a function of luminosity. A best fit line has a slope of only -0.017. The ratio should be 2.32 for a perfect exponential disk.

seen that the low dynamic range in ΔV will always make it difficult to find the exponent α accurately, and it makes more sense to incorporate ΔV into the Dynamical Mass ($\equiv$ R ΔV^2) instead, as it is in Gavazzi's Law (C) where it leads to both a clear correlation with Luminosity (Fig. 20) and perhaps a natural physical explanation ['all galaxies are made of the same stuff'].

The distance to most galaxies in our radial velocity range can be problematic so it is important to ask if and how distance uncertainties will affect the correlations. Where there is a difference (last column) between the distance-dependant exponents x in our list one expects distance uncertainties to introduce extra scattering to correlations, as for instance in (A) but not in (E). It is interesting to note that the tightest correlations observed i.e. (D) and (E) are the ones unaffected by distance uncertainties, whilst the loosest, i.e. (A) [Fig. 15] and (B) [Fig. 16] should indeed be the strongest affected. This hints that distance uncertainties probably are increasing the scatter. On the other hand look at Gavazzi's relation (B) and in particular Figures 17 and 20. There is no increase in scatter when we come to lower radial velocities where one might expect the relative distance-uncertainties to have the most pernicious effect on the correlations. This suggests that although distance uncertainty can increase scatter, that increase must be rather limited here, and exculpates the uniform but rather crude distances we have adopted. Note also that only 1 observable is size, and hence distance dependant (R $\equiv d\theta_{90}$) while 5 are not, i.e. $\Sigma_{opt}, N_{HI}, (g-r), \Delta V$ and Concentration R_{90}/R_{50}. This implies strong correlations among *intrinsic* galaxy properties (e.g. colour and SB, ΔV and N_{HI}) i.e. ones that have nothing to do with either scale or distance.

How constraining could the five discussed correlations (A) to (E) be on theories of galaxy formation and evolution? That depends on how many fundamental, independent invariant physical properties galaxies might posses. At present it is hard to imagine more than 7: total mass, baryon fraction, age, angular momentum, random energy, radius and central condensation. Once a galaxy has virialised, the Virial Theorem will provide one relation between them, leaving only 6 independent properties. Ignoring interactions one might expect, to first order, that these properties might be conserved by each galaxy though, on a secular time-scale some random energy might be dissipated, while some baryons might be ejected. Thus five correlations (if they are truly independent) within a six-parameter set hint at a high degree of organisation among gas-rich galaxies, something partially foreshadowed by the early HI pioneers [Brosche 1973, Balkowski 1973]. We are presently carrying out a Principal Component Analysis to investigate the degree of organisation in this data.

On the observational front work in progress by us includes enlarging the sample size as more SDSS and HI data [e.g. from the Bonn 100 metre Multibeam Survey (Kerp et al. in preparation) becomes available. Our automated SDSS photometric pipeline for large galaxies should greatly accelerate progress (West et al. 2008). HI interferometry is being obtained, first to sort out identifications in tight groups and second to measure more actual HI radii to get a better understanding of the Minchin-Rosenberg effect. So far we have exploited neither the colours nor the fibre spectra but work is in hand to include them too (West et al. in preparation). Statistical work on mean cosmic properties, such as the mean HI cosmic density, depends on a clear understanding of ones selection effects and this is underway too (Garcia-Appadoo et al. in preparation). We are also working on the reverse List, that is to say a list of objects in the SDSS survey which we would have expected to contain measurable HI, and thus show up in the Equatorial Survey, but which do not (West & Garcia-Appadoo in preparation).

ACKNOWLEDGMENTS

MJD would like to thank the UK Particle Physics and Astronomy Research Council (PPARC) for grants towards the support of both construction and exploitation of the HIPASS and HIJASS (HIPASS Northern equivalent at Jodrell Bank) surveys, and especially thank the HIPASS team, notably Professors Lister Staveley-Smith, Ron Ekers and Dr A. E. Wright of the Australia Telescope at CSIRO Radiophysics in Sydney, for the inspiration and drive which first got the Multibeam project going.

This publication makes use of data products from the Two Micron All Sky Survey, which is a joint project of the University of Massachusetts and the Infrared Processing and Analysis Center/California Institute of Technology, funded by the National Aeronautics and Space Administration and the National Science Foundation.

Funding for the SDSS and SDSS-II has been provided by the Alfred P. Sloan Foundation, the Participating Institutions, the National Science Foundation, the U.S. Department of Energy, the National Aeronautics and Space Administration, the Japanese Monbukagakusho, the Max Planck Society, and the Higher Education Funding Council for England. The SDSS Web Site is http://www.sdss.org/.

The SDSS is managed by the Astrophysical Research Consortium for the Participating Institutions. The Participating Institutions are the American Museum of Natural History, Astrophysical Institute Potsdam, University of Basel, University of Cambridge, Case Western Reserve University, University of Chicago, Drexel University, Fermilab, the Institute for Advanced Study, the Japan Participation Group, Johns Hopkins University, the Joint Institute for Nuclear Astrophysics, the Kavli Institute for Particle Astrophysics and Cosmology, the Korean Scientist Group, the Chinese Academy of Sciences (LAMOST), Los Alamos National Laboratory, the Max-Planck-Institute for Astronomy (MPIA), the Max-Planck-Institute for Astrophysics (MPA), New Mexico State University, Ohio State University, University of Pittsburgh, University

of Portsmouth, Princeton University, the United States Naval Observatory, and the University of Washington.

REFERENCES

Abazajian K. et al., 2004, AJ, 128, 502
Abazajian K. et al., 2005, AJ, 129, 1755
Balkowski C., 1973, A&A, 29, 43
Barnes D.G. et al., 2001, MNRAS, 322, 486
Begum A., Chengalur J.N., Karachentsev I.D., Kaisin S.S., Sharina M.E., 2006, MNRAS, 365, 1220
Bingelli B., Sandage A., Tarenghi M., 1984, AJ, 89, 64
Binney J., Merrifield M., 1998, Galactic Astronomy, Princeton University Press
Blanton M.R. et al., 2001, AJ, 121, 2358
Blanton M.R. et al., 2003, ApJ, 592, 819
Bosma A., 1978, PhD Thesis, University of Groningen
Braun R., 1997, ApJ, 484, 637
Brosche P., 1973, A&A, 23, 259
Bruzual G. & Charlot S., 2003, MNRAS, 344, 1000
Cawson M.G.M., Kibblewhite, E.J., Disney, M.J., Phillipps, S., 1987, MNRAS, 224, 557
Cross N. J. G., et al. 2004, MNRAS, 349, 576
Dalcanton J.J., Spergel D.N., Gunn J.E., Schmidt M., Schneider D.P., 1997, AJ, 114, 2178
Davies J.I., Sabatini S., Roberts S., 2004, PASA, 21, 360
Davies J.I., Disney M.J., Minchin R.F., Auld R.F., Smith R., 2006, MNRAS, 368, 1479
de Vaucouleurs G., de Vaucouleurs A., Corwin H.G., Buta, R.J., Paturel G., Fouque P., 1991, MNRAS, 249, 28
Disney M.J., 1976, Nature, 263, 573
Disney M.J., Phillipps, S., 1983, MNRAS, 205, 1253
Disney M.J., Banks G., 1997, PASA, 14, 69
Disney M.J., 1999, in Low Surface Brightness Universe, ASP Conference Series 170, Edited by J.I. Davies, C. Impey, and S. Phillipps. Astronomical Society of the Pacific (San Francisco), pp. 9-18
Disney M.J., Minchin R.F., 2003, in The IGM/Galaxy Connection: The Distribution of Baryons at $z = 0$, ASSL Conference Proceedings Vol 281., Edited by Jessica L. Rossenberg and Mary E. Putman
Disney M.J., 2008, "Dark Galaxies and Lost Baryons", IAU Symposium 244, CUP, p1
Doyle M.T., Drinkwater M.J., 2006, MNRAS, 372, 977
Fisher J.R., Tully R.B., 1981, ApJ, 243, 23
Fixsen D.J., Cheng E.S., Gales J.M., Nather J.C., Shafer R.A., Wright E.L., 1996, ApJ, 473, 576
Freeman K.C., 1970, ApJ, 160, 811
Fukugita M., Hogan C.J., Peebles P.J.E., 1998, ApJ, 503, 518
Garcia-Appadoo D.A., 2005, The Equatorial Strip - A blind HI survey for gas-rich galaxies, PhD Thesis, Cardiff University
Gavazzi G., Pierini D., Boselli A., 1996, A&A, 312, 397
Gavazzi G., Boselli A., Donati A., Franzetti P., Scodeggio M., 2003, A&A, 400, 451
Giovanelli R., Haynes M.P., 1989, ApJL, 346, 1989
Giovanelli R. et al., 2005, AJ, 130, 2613
Grossi M. et al., 2007, MNRAS, 374, 107
Hambly N.C. et al., 2001, MNRAS, 326, 1279
Holmberg E., 1965, ArA, 3, 387
Hubble E., 1937, MNRAS, 97, 506
Huchtmeier W.K., Richter O.G., 1998, A&A, 203, 237
Impey C., Bothun G., 1997, ARA&A, 35, 267
Karachentsev I.D., Makarov D.A., 1996, AJ, 111, 794
Kennicut R.C.Jr., ApJ, 344, 685
Kilborn, V.A., 2002, AJ, 124, 690
Kovac K, 2007, PhD Thesis, University of Groningen
Leitherer C. et al., 1999, ApJS, 123, 3
McGaugh S.S., Bothun G.D., 1994, AJ, 107, 530
Meyer M.J. et al., 2004, MNRAS, 350, 1195
Minchin R.F. et al., 2003, MNRAS, 346, 787
Minchin R.F. et al., 2004, MNRAS, 355, 1303
Minchin R.F. et al., 2005, A&AS, 37, 1483
Minchin R.F. et al., 2007, ApJ, 670, 1056
Roberts M.S., Haynes M.P., 1994, ARA&A, 32, 115
Rosenberg J.L., Schneider S.E., 2000, ApJS, 130, 177
Rosenberg J.L., Schneider S.E., 2003, ApJ, 585, 256
Rosenberg J.L., Schneider S.E., Posson-Brown J., 2005, AJ, 129, 1311
Salpeter E.E., Hoffman G.L., 1996, ApJ, 465, 595
Salzer J.J., di Serego Akighieri S., Matteucci F., Giovanelli R., Haynes M., 1991, AJ, 101, 1258
Schaye J., 2008, "Dark Galaxies and Lost Baryons", IAU Symposium 244, CUP, p247
Shostak G.S., 1977, A&A, 54, 919
Skrutskie M.F. et al., 2006, AJ, 131, 1163
Spitzak J.G., Schneider S.E., 1998, ApJS, 119, 159
Sprayberry D., Impey C.D., Irwin M.J., McMahon R.G., Bothun G.D., 1993, ApJ, 417, 114
Staveley-Smith L., 1996, PASA, 13, 243
Strateva I. et al., 2001, AJ, 122, 1861
Swaters R.A., Madore B.F., van den Bosch F.C., Balcells M., 2003, ApJ, 583, 732
Tully R.B., Fisher J.R., 1977, A&A, 54, 661
Tully R.B., Fisher J.R., 1981, ApJS, 47, 139
West A.A., 2005, HI selected galaxies in the Sloan Digital Sky Survey, PhD Thesis, University of Washington
West A.A., et al., 2008, AJ, submitted
Wong O.I. et al., 2005, MNRAS, 371, 1855
Zwaan M.A., Briggs F.H., Sprayberry D., Sorar E., 1997, ApJ, 490, 173
Zwaan M.A. et al., 2004, MNRAS, 350, 1210
Zwicky F., 1942, PASP, 54, 185Z